



Efficient Multi-Composite Cement Made of Granulated Blast Furnace Slag (GBFS) and Flash-calcined Sediment

Mahfoud Benzerzour^{1, 2}, Duc Chinh Chu^{1, 2*}, Mouhamadou Amar^{1, 2},
Joelle Kleib^{1, 2}, Nor-Edine Abriak^{1, 2}, Jaouad Nadah³

¹ Centre for Materials and Processes, Institut Mines-Télécom, IMT Nord Europe, F-59508 Douai, France.

² Laboratoire de Génie Civil et Géo-Environnement, ULR 4515—LGCgE, Institut Mines-Télécom, University Lille, F-59000 Lille, France.

³ EQIOM LeLAB, CRT 1 Parc Vendôme-460 Allée de l'Innovation, 59810 Lesquin, France.

Received 27 May 2023; Revised 08 October 2023; Accepted 17 October 2023; Published 01 November 2023

Abstract

The objectives of this study were to find out in detail how well granulated blast furnace slag (GBFS) could be replaced by flash-calcined sediment (SF sediment) in terms of hydration kinetics and mechanical-microstructural properties when developing an eco-friendly cement binder. The results indicated that the SF sediment substitution with a rate of 25% wt significantly improved the hydration kinetics of cement compared to the reference. This contributed to a considerable enhancement of the mechanical-microstructural properties of the mortar containing the SF sediment. By comparison with the reference, the strength of multi-composite cement-based mortar increased by 33% at 2 days and by 4.5% at 28 days, whereas its porosity decreased by 16.32% and by 12.44% for the same period. The SEM-EDS result showed that the SF sediment substitution did not significantly modify the chemical composition of the C-S-H phase, with a Ca/Si ratio range of 1.82 to 2.84 for both cement pastes. Moreover, Mg²⁺ and Al³⁺ ions were two principal elements incorporated in C-S-H gels, with different ratios depending on the Ca/Si ratio of C-S-H gels. A novel model established from a combination of the curve fitting method and Power's approach allowed for accurate prediction of the strength development of multi-composite cement-based mortars. Overall, the SF sediment substitution could be considered a promising option to develop a more eco-friendly cement binder, while the novel approach could be used as a reliable model for the strength prediction of blended cement.

Keywords: Flash-calcined Sediment; Pozzolanitic; Cement; Hydration; Compressive Strength Prediction; Porosity.

1. Introduction

Cement is an indispensable and essential component for concrete production, with approximately 4.6 billion tons produced in 2022. However, cement production is responsible for 7% of global CO₂ emissions, principally due to the CO₂ released during clinker production [1]. Thus, reducing Portland cement clinker content becomes one of the key objectives of the cement industry to reduce CO₂ emissions as well as reserve natural resources. Numerous alternative materials, such as limestone [2–5], granulated blast furnace slag (GBFS) [6, 7], fly ash (FA) [8], silica fume (SF) [9], and metakaolin [10], have been used as supplementary cementitious materials (SCMs) to replace a part of ordinary Portland cement. From an environmental point of view, the efficient use of SCMs not only significantly reduces clinker content in cement but also solves the disposal issue for the storage of some industrial residual products. From a technical point of view, a remarkable improvement in the mechanical and durability properties has been observed, especially for concrete containing GBFS and fly ash [11–13].

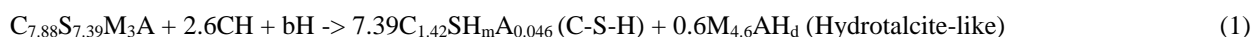
* Corresponding author: duc.chinh.chu@imt-nord-europe.fr

 <http://dx.doi.org/10.28991/CEJ-2023-09-11-02>



© 2023 by the authors. Licensee C.E.J, Tehran, Iran. This article is an open access article distributed under the terms and conditions of the Creative Commons Attribution (CC-BY) license (<http://creativecommons.org/licenses/by/4.0/>).

GBFS is an amorphous material formed from steel production by thermochemical reduction in a blast furnace [14]. The chemical composition of GBFS consists generally of CaO, SiO₂, Al₂O₃, and MgO oxides [15]. When GBFS is added to ordinary Portland cement (OPC), GBFS has reacted with Ca(OH)₂ produced by cement hydration to form calcium-silicate-hydrates (C-S-H) [16], which is of fundamental importance for the strength development and durability of the concrete [17]. From a chemical point of view, the hydration reaction of GBFS containing CaO, SiO₂, MgO, and Al₂O₃ with a molar proportion of 7.88: 7.39: 3:1, respectively, in the presence of Ca(OH)₂ can be written according to Equation 1, as proposed by Richardson et al. [18]:



Where, $7.39m + 0.66d = b$.

By comparison with C-S-H produced from OPC hydration, a decrease in the Ca/Si ratio and an increase in the Al/Ca ratio of C-S-H gels lead to a change in the C-S-H morphology, resulting in a densification of the microstructure [19]. In terms of durability properties, the addition of GBFS to cement has significantly reduced the chloride ion migration due to the chloride binding and formation of Friedel's salt. For this reason, slag cement (CEM III cement, as described in EN 197-1 [20]) has been widely used in the last few decades. However, it should be noted that more than 80% of the worldwide available GBFS has already been used as SCMs or concrete addition [21], so all the potential materials must be investigated to reduce the demand for GBFS in cement and concrete. A possible solution could be multi-composite cement using a moderate amount of GBFS in combination with other components [6]. One of the potential materials that has been studied as SCMs in recent years is the sediment obtained by dredging operations, with approximately 56 Mm³ and 300 Mm³ of sediment dredged in France and Europe, respectively [22]. Raw sediments generally have a high organic matter content [23, 24], which can obviously change the cement hydration [25], leading to an increase in porosity and a loss of compressive strength [26, 27]. Mineralogically, raw sediments generally contain quartz (SiO₂), calcite (CaCO₃), and clay phases including kaolinite, illite, and smectite [28], so heat treatment methods have often been used to eliminate the organic matter as well as transform non-reactive kaolinite (Al₂O₃(SiO₂)₂·2H₂O) into amorphous reactive metakaolin (Al₂O₃(SiO₂)₂) [29, 30].

Two essential calcination methods have been often used for sediment treatment, such as traditional calcination in a furnace [31–33] and flash calcination [28]. Calcined sediments use as SCMs has been extensively investigated in previous studies. The results indicated that the calcined sediment significantly improved the hydration kinetics [24], mechanical properties, and properties of mortar and concrete [34], compared with raw sediment. Nevertheless, due to the long time and high temperature of the calcination process (generally, 1-3 hours at 800-850 °C [32, 35]), the traditional calcination method is seldom used for sediment treatment in large quantities from an economical point of view. In comparison with the conventional calcination method, the flash calcination method presents numerous advantages, including a much shorter calcination time, better temperature control, lower energy consumption, and higher reactivity [36]. In addition, the energy consumed by the flash calcination method is approximately 2 GJ per ton of sediment [37], which is similar to the energy required for the production of 1 ton of GBFS (1.9770 GJ per ton of GBFS [38]). Thus, GBFS replacement by flash-calcined sediment in slag cement production can be considered a promising solution in terms of environmental impact.

1.1. Significance and Originality

Although the use of flash-calcined sediment as a replacement for GBFS and metakaolin (MK) in cementitious materials was investigated in previous studies [39, 40], the impacts of flash-calcined sediment substitution on the hydration kinetics, the formation of hydration products, and the potential change in the composition of hydrates were not studied. In addition, in these studies, the supplementary cementitious materials were directly mixed with the cement; this could lead to a potential change in the particle size distribution of blended cement, affecting the hydration and the development of mechanical-microstructural properties of mixtures.

Hence, this study filled several gaps found in the previous research. The influences of flash-calcined sediment for a partial BGFS replacement on the properties of multi-composite cement, including the hydration kinetics, hydration products, and their chemical composition, as well as mechanical-microstructural development, were investigated on the blended cements having the same particle size distribution. Additionally, a novel approach was also established to predict the compressive strength development of multi-composite cement-based mortar. This was of utmost importance in practical application because the prescriptive approaches of the concrete industry, based mainly on experience obtained with ordinary Portland cement, will not be applicable to the new multi-composite cement. The process of the methodology used in this research is summarized in Figure 1.

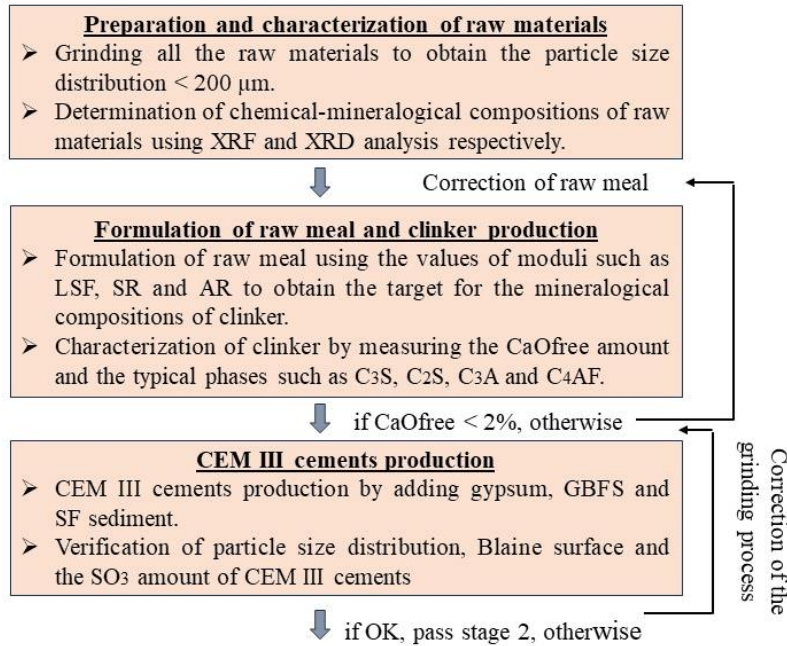
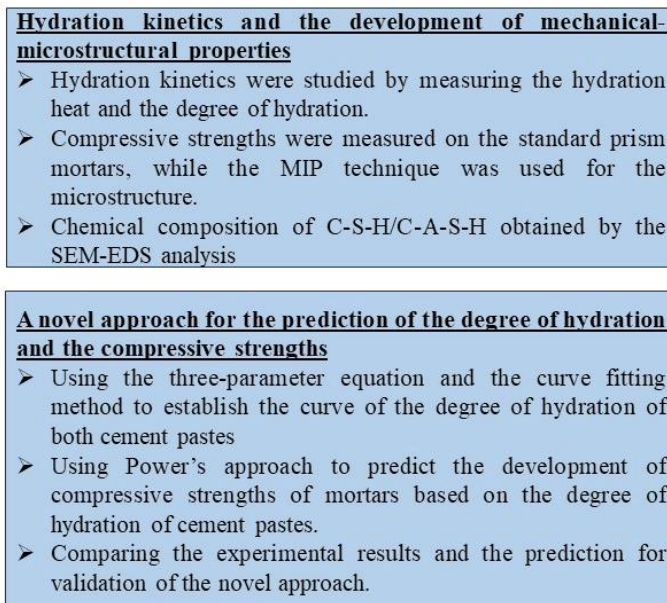
Stage 1: Production of CEM III cement in the laboratory**Stage 2: Investigating the efficiency of SF sediment for the development of mechanical-microstructural properties and a novel approach for the prediction of strength development**

Figure 1. Schematic diagram for the process of the methodology

2. Production and Characterization of Anhydrous Multi-composite Cements**2.1. Raw Materials and Multi-composite Cement Production Method**

Contrary to previous studies [6, 7], which mixed OPC directly with different SCMs to produce the multi-composite cement, this could impact the hydration due to the change in surface area and granulometry of blended cement during grinding. For this reason, in this study, CEM III cements were produced in the laboratory by grinding components such as clinker, GBFS, flash-calcined sediment and gypsum. This allowed us to avoid the potential changes in granulometry and optimize SO₃ content in CEM III cements. Clinker was first produced from conventional raw materials including limestone, clay, sand, and iron oxide. These materials were dried to a constant mass and ground finely before characterization. The proportion of each raw material in the raw mixture was determined to achieve the targeted mineralogical composition of clinker. Based on the chemical composition of all raw materials obtained by X-ray fluorescence (XRF) analysis, a raw mixture was formulated using the following moduli values: Lime Saturation Factor (LSF), Silica Ratio (SR) and Alumina Ratio (AR) respectively. The three moduli are given in the following equations:

$$LSF = \frac{\% \text{CaO}}{2.8 * \% \text{SiO}_2 + 1.20 * \% \text{Al}_2\text{O}_3 + 0.65 * \% \text{Fe}_2\text{O}_3} \tag{2}$$

$$SR = \frac{\% \text{SiO}_2}{\% \text{Al}_2\text{O}_3 + \% \text{Fe}_2\text{O}_3} \tag{3}$$

$$AR = \frac{\% \text{Al}_2\text{O}_3}{\% \text{Fe}_2\text{O}_3} \tag{4}$$

In the cementitious industry, the values of these moduli are variable between 92 and 102 for LSF, 2 and 3 for SR, 1 and 4 for AR, depending on the chemical composition of raw materials as well as the mineralogical composition required of cement. In this study, the proportion of raw materials in the mixture was calculated using the following values: LSF = 98, SR = 2.6, and AR = 1.45, respectively. The chemical composition and proportion of each component in the raw mixture are given in Table 1.

Table 1. Chemical composition and proportion of raw materials in the raw meal

Oxide (wt%)	Limestone 1	Limestone 2	Limestone 3	Clay 1	Clay 2	Sand	Iron oxide
SiO ₂	5.3	9.5	6.0	48.7	60.6	88.3	2.2
Al ₂ O ₃	1.9	3.7	1.2	20.6	14.9	4.8	0.3
Fe ₂ O ₃	0.6	1.3	0.6	10.7	7.9	1.2	70.6
CaO	49.8	45.8	50.0	1.1	2.3	2.1	13.5
MgO	0.4	0.6	0.4	1.1	0.8	ND	2.2
Na ₂ O	ND	ND	ND	ND	ND	ND	ND
K ₂ O	0.4	0.9	0.2	1.5	1.3	0.3	0.1
SO ₃	ND	ND	ND	ND	ND	ND	0.2
TiO ₂	ND	0.1	ND	0.7	0.7	0.9	ND
P ₂ O ₅	ND	ND	0.2	0.3	0.2	ND	ND
Mn ₂ O ₃	ND	ND	ND	ND	0.2	ND	0.7
ZnO	ND	ND	ND	ND	ND	0.1	ND
L.O.I	40.9	37.5	40.9	14.6	10.5	1.9	10.2
Total	99.3	99.4	99.5	99.3	99.4	99.6	98.7

Raw mixture composition							
Raw material	Limestone 1	Limestone 2	Limestone 3	Clay 1	Clay 2	Sand	Iron oxide
(wt.%)	52.08	17.36	17.36	3.18	4.78	4.31	0.93

-ND: Not detected; L.O.I: Loss of ignition.

The process of clinker production in the laboratory is described in previous studies [41, 42] and summarized in Figure 2.

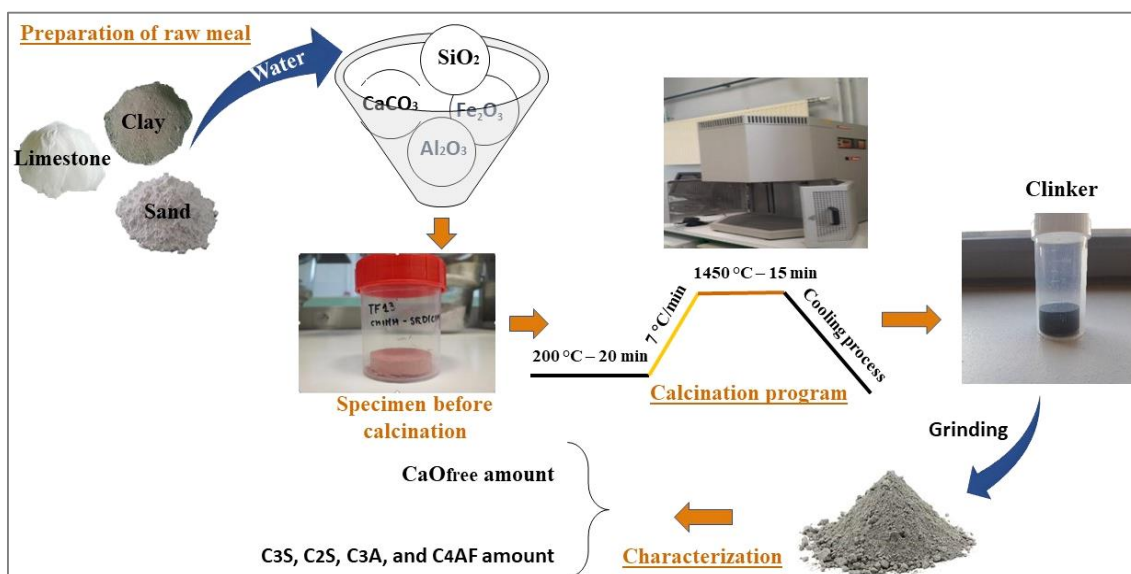


Figure 2. Schematic diagram for the process of the clinker production

After mixing all the raw components through a wet process to better homogenize the meal, this raw mixture was calcined in a static kiln with the same heating process used in the previous studies [41, 42]. The clinker was then characterized to investigate the quality of the clinkering process. The free lime (CaO_{free}) amount of clinker was determined using the Schlafer-Bukolowki method [43], whereas the crystalline phases were detected using X-ray diffraction (XRD) analysis. The chemical composition of clinker was obtained by X-ray fluorescence (XRF) analysis, and the mineralogical phase amount was calculated using Bogue's formula. The results are given in Table 2.

Table 2. Mineralogical-chemical composition of clinker

Mineralogical composition of clinker												
Mineralogical phase	C_3S (wt. %)	C_2S (wt. %)	C_3A (wt. %)	C_4AF (wt. %)	CaO_{free} (wt. %)	Total (wt. %)						
	61.63	15.76	9.14	9.18	1.60	97.31						
Chemical composition of clinker												
Oxide	CaO	SiO_2	Al_2O_3	Fe_2O_3	SO_3	Na_2O	K_2O	MgO	ZnO	P_2O_5	L.O.I	Total
Exp	65.19	21.05	5.22	2.93	0.03	ND	0.71	0.72	0.03	0.18	3.0	99.40
Target	67.91	21.71	5.41	3.28	ND	ND	0.83	0.75	0.02	0.09	0.0	100

It can be seen that CaO_{free} content of clinker is lower than the threshold value of 2 wt.% that is generally required in the cement industry. This confirms that the clinkering process was complete and that the cooling process didn't lead to the decomposition of C_3S into C_2S and CaO_{free} .

Sediment was previously treated by the flash-calcination method at a temperature of 750 °C. The characteristics of flash-calcined sediment (hereafter SF sediment) were analyzed and detailed in a previous study [24]. Granulated blast furnace slag (GBFS) and gypsum were provided by the EQIOM company. The specific surface area of SF sediment and GBFS was measured using the BET (Brunauer-Emmett-Teller) method, while XRF analysis was used to determine the chemical composition of the materials. The results are given in Table 3.

Table 3. Physical properties and chemical composition of GBFS, SF sediment and gypsum

Chemical composition	SF sediment	GBFS	Gypsum
SiO_2	49.71	34.27	1.95
Al_2O_3	12.00	10.96	0.33
Fe_2O_3	5.33	0.27	0.28
CaO	11.21	40.98	32.85
MgO	1.12	6.56	0.34
Na_2O	0.74	0.17	ND
K_2O	2.25	0.49	0.08
SO_3	0.18	0.43	38.58
ZnO	0.31	ND	ND
P_2O_5	2.26	ND	ND
L.O.I	13.70	4.70	24.85
Total	98.81	99.40	99.26
Physical properties			
Specific density (g/cm^3)	2.65	2.88	2.33
BET surface area (m^2/g)	15.59	2.7	-

The main oxides of SF sediment and GBFS are CaO, SiO_2 , Al_2O_3 , Fe_2O_3 and MgO. However, the proportion of these oxides in SF sediment and GBFS is very different. SF sediment contains more SiO_2 but significantly less CaO than GBFS. The MgO content of SF sediment is six times less, whereas the Fe_2O_3 content of SF sediment is twenty times higher than that of GBFS. Thus, GBFS replacement by SF sediment can lead to a reduction of hydrotalcite-like phase content in cement containing SF sediment. In addition, SF sediment exhibits a BET surface area six times higher than GBFS.

The mineralogical composition of SF sediment and GBFS was studied using XRD analysis and presented in Figures 3(a & b) respectively. The main mineralogical phases of SF sediment are quartz, calcite, anhydrite, and illite/muscovite, whereas GBFS contains principally the amorphous. In addition, the transformation of kaolinite to metakaolin in SF sediment after flash calcination was demonstrated in a previous study [24].

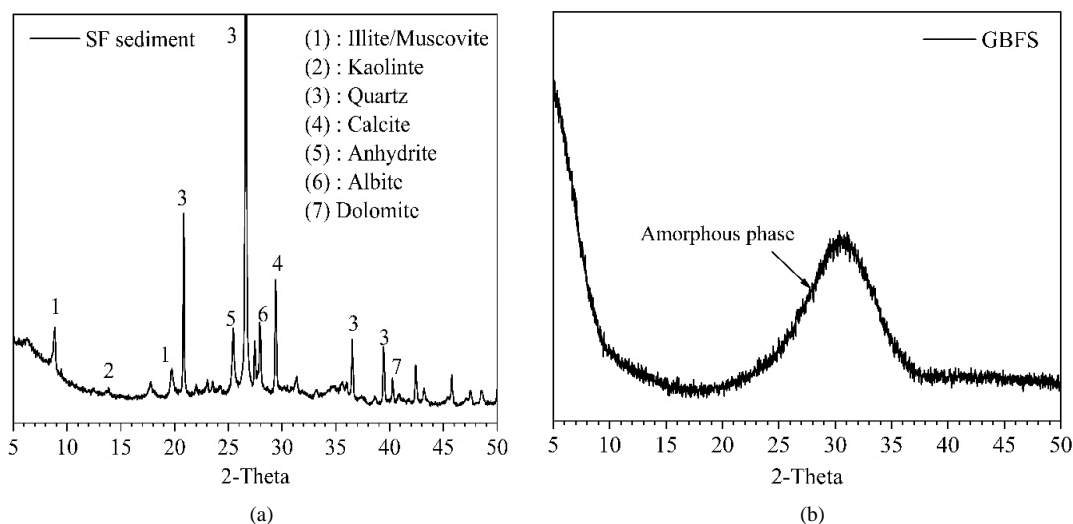


Figure 3. XRD patterns. (a): SF sediment, (b): GBFS

Due to the limited amount of clinker that could be made in the lab, the consistency of cement pastes was tested with different substitution rates of GBFS by SF sediment, ranging from 25% to 75%. The goal was to determine an appropriate incorporation ratio of SF sediment while assuming the workability requirement. The result indicated that the workability of cement pastes decreased with an increase in the SF sediment content. Consequently, a substitution ratio of 25% of SF sediment was selected for the next parts of the study. Finally, two CEM III cements were produced with and without SF sediment in the laboratory. The first one is the reference cement (hereafter CEM III Ref) made from clinker, GBFS, and gypsum only. The second one is named CEM III SF and is produced from clinker, GBFS, SF sediment, and gypsum. SF sediment was used as a substitution for 25 wt.% of GBSF in the CEM III cement. Gypsum was added to obtain a SO₃ amount of 2.4 wt.% in both cements. The composition of both CEM III cements is given in Table 4. All components were ground in a centrifugal ball mill until they achieved a Blaine-specific surface area of 3500 cm²/g.

Table 4. Proportion of individual component in CEM III cements

Cement	Clinker (wt.%)	GBFS (wt.%)	SF sediment (wt.%)	Gypsum (wt.%)
CEM III Ref	56.55	37.70	-	5.76
CEM III SF	56.48	28.24	9.41	5.86

2.2. Anhydrous Cements Characterization

Prior to studying the hydration kinetics, two anhydrous CEM III cements were characterized using different methods. The specific surface area was measured using two different methods: the Blaine surface method according to NF EN 196-6 and the BET surface area method according to NF EN ISO 18757. The density of cements was determined using a helium pycnometer, the Accupyc 1330 device. The water demand as well as the initial setting time of cements were measured using a Vicat instrument, according to NF EN 196-3 [44]. The characteristics of anhydrous CEM III cements are given in Table 5.

Table 5. Physical characteristics of both CEM III cements

Property	CEM III Ref	CEM III SF
Density (g/cm ³)	3.02	2.98
Blaine-specific surface (cm ² /g)	3860	3980
BET-specific surface (m ² /g)	1.37	1.90
Water demand (%)	33.33	35.00
Setting time (minutes)	255	280

The specific density of CEM III SF cement is slightly lower than that of CEM III Ref cement. It is due to a lower specific density of SF sediment compared to that of GBFS (2.65 g/cm³ for SF sediment and 2.88 g/cm³ for GBFS). The BET-specific surface area of CEM III SF is much higher than that of CEM III Ref. An increase in BET surface area could lead to an increase in water demand and the initial setting time of CEM III SF cement compared with the reference as indicated in previous studies [39, 32, 45]. The curve of particle size distribution of both cements is shown in Figure 4. It can be seen that the particle size distribution for both cements is very similar. This indicated that the grinding process used in this study is adequate.

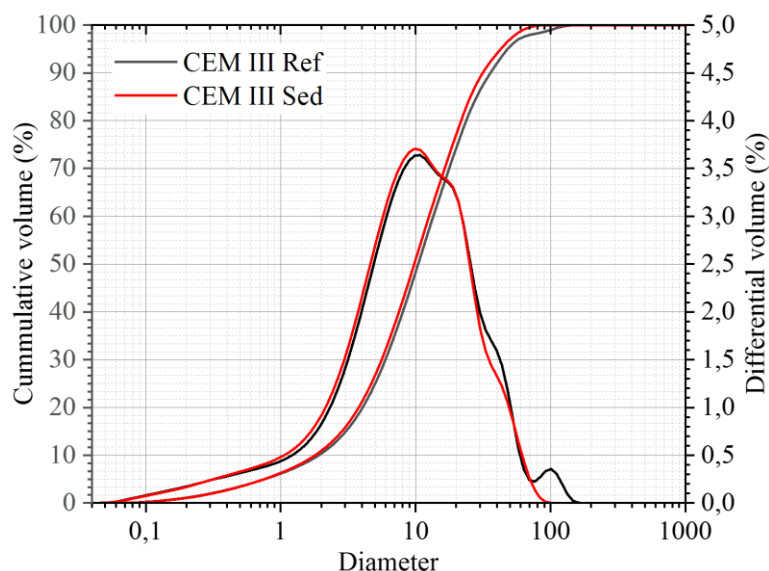


Figure 4. Particles size distribution of CEM III Ref and CEM III SF cements

The chemical composition of CEM III cements was measured using XRF analysis to check the SO_3 amount in cements. The result is in Table 6.

Table 6. Chemical composition of two cements measured by XRF analysis

Cement	CaO	SiO ₂	Al ₂ O ₃	Fe ₂ O ₃	SO ₃	Na ₂ O	K ₂ O	MgO	ZnO	P ₂ O ₅	LOI	Total
CEM III Ref	54.20	24.94	7.10	1.77	2.31	0.07	0.59	2.90	0.02	0.10	4.90	99.35
CEM III SF	51.37	26.36	7.19	2.25	2.35	0.12	0.75	2.39	0.05	0.31	5.77	99.29

It can be seen that the SO_3 content in both cements is close to the targeted value of 2.4 wt.%. This is of utmost importance to investigate the cement hydration kinetics because SO_4^{2-} concentration strongly influences the hydration rate of cement phases, particularly in the case of C_3A and C_3S [46]. As expected, SF sediment substitution increased SiO_2 content and decreased CaO and MgO contents in CEM III SF cement. The CaO/ SiO_2 ratio decreased from 2.328 in CEM III Ref to 2.087 in CEM III SF cement.

3. Characterization of Hydrated Cements

Multi-technique approaches were used to study the hydration as well as mechanical-microstructural properties of CEM III cements, including isothermal conduction calorimetry, thermogravimetric, mercury intrusion porosimetry (MIP), XRD analysis, scanning electron microscopy coupled with Energy Dispersive X-ray (SEM-EDS), and compressive strength tests.

3.1. Hydration Kinetics of CEM III Cements

Since cement hydration reactions are an exothermal process [16], the variation in the heat released during hydration may provide information on potential changes in the hydration rate or imply a modification in the hydration mechanisms of cement. Isothermal conduction calorimetry analysis was used to follow the heat flux liberated from the hydration reactions of cement pastes. For this measurement, cement pastes made with a water-to-cement ratio of 0.5 were mixed for 2 minutes at 1600 rpm, then poured into a cell placed in a calorimeter. This analysis was performed at a constant temperature of 20 °C, and the hydration heat was measured for 72 hours.

For other analyses, including TGA, XRD, and SEM-EDS, cement pastes were prepared with a water-to-cement ratio of 0.5 according to the following process. After mixing for 5 minutes at 1600 rpm, the pastes were poured into a small container and rotated for 6 hours in order to avoid the segregation and blending of cement. After 24 hours, cement pastes were demolded and cured in a saturated lime solution at a constant temperature of 20 °C. For TGA, XRD, and SEM-EDS analyses, the cement hydration was stopped using the solvent exchange method (isopropanol solvent [47]). After immersing in the solvent solution for 3 days, samples were stored in a desiccator under a slight vacuum for at least 7 days to evaporate the solvent.

TGA was used to quantify the Portlandite ($\text{Ca}(\text{OH})_2$) and chemically bound water amounts produced by the cement hydration. 100 mg of powdered sample ($<63 \mu\text{m}$) was analyzed using the Netzsch STA 409 device with a heating rate of 3 °C/min from 40 °C to 1000 °C under constant nitrogen flow. $\text{Ca}(\text{OH})_2$ amount was quantified using the tangent

method [48], while the chemically bound water content was obtained from the mass loss of sample between 40 °C and 460 °C. For comparison, these contents were normalized per 100 g of anhydrous cement according to Equation 5 and 6.

$$W_b(t) = \frac{M_{\text{sample}}(40\text{ }^\circ\text{C}) - M_{\text{sample}}(460\text{ }^\circ\text{C})}{M_{\text{sample}}(460\text{ }^\circ\text{C})} \times 100 \quad (5)$$

$$CH = \frac{M_{\text{sample}}(400\text{ }^\circ\text{C}) - M_{\text{sample}}(460\text{ }^\circ\text{C})}{M_{\text{sample}}(460\text{ }^\circ\text{C})} \times \frac{M_{\text{Ca(OH)}_2}}{M_{\text{H}_2\text{O}}} \times 100 \quad (6)$$

where $M_{\text{sample}}(40\text{ }^\circ\text{C})$, $M_{\text{sample}}(400\text{ }^\circ\text{C})$, $M_{\text{sample}}(460\text{ }^\circ\text{C})$ are Mass of sample at 40 °C, 400 °C and 460 °C respectively. $M_{\text{Ca(OH)}_2}$, $M_{\text{H}_2\text{O}}$ are Molar mass of Portlandite (74 g/mol) and water (18 g/mol) respectively.

X-ray diffraction (XRD) analysis was carried out to identify the hydrate products of cement. Hydration-stopped pastes were ground manually to obtain a smaller particle size than 40 μm . Then, the sample was analyzed using a Bruker D2 Advance diffractometer. This instrument is equipped with a Cu anode with $\lambda = 1.5406\text{ \AA}$ and operated at 40 kV-40mA conditions. The sample was analyzed with the 2θ angle scanned from 5° to 80° and a step size of 0.02° and 1s per step.

The chemical composition of the C-S-H gels of cement pastes after 28 days of hydration was measured using the SEM-EDS technique. Hydration-stopped pastes were cut into 2 mm-thick slices, then impregnated under vacuum using the epoxy. Samples were polished using a diamond suspension with deodorized petroleum as lubricant. Between each step in the process, samples were cleaned using isopropanol. After 2 days in a desiccator under vacuum to remove the remaining isopropanol, cement pastes were coated with carbon to make the surface conductive and enable SEM analysis at high vacuum [49]. The Hitachi S-4300SE/N was used with an accelerating voltage of 20 kV and a current of 0.8 nA. 100 points per sample were measured in different zones to obtain a representative result for the chemical composition of C-S-H gels.

3.2. Mechanical-microstructural Properties of Mortars

3.2.1. Compressive Strength

The classification of cements was determined based on the compressive strength of standard mortars according to NF EN 197-1 [20]. Prism mortar samples (40 x 40 x 160 mm³) were made according to NF EN 196-1 [50] and cured under saturated conditions at a constant temperature of 20 °C. The compressive strength of mortars was measured after 2, 7, and 28 days of curing using an INSTRON 5500R device, which has a maximum applicable load of 150 kN with a displacement rate of 144 KN/min.

3.2.2. A Novel Approach for Prediction of Compressive Strength Development of Multi-composite Cement-based Mortars

Strength development with time is one of the essential parameters to investigate the efficiency of mineral addition on cement hydration. However, experimental measurement usually requires much time and materials for sample preparation. Thus, several predictive models established by Féret, Bolomey and Abrams as described in previous studies [51–53] have been used to predict the strength development of mortar or concrete. In a previous study [53], different formulas were used to predict the compressive strength of sediment-based mortars. However, the results indicated that these models were not adapted for predicting the strength of multi-composite cement-based mortars. For this reason, in this study, a novel approach was established using Power empirical relation to predict the strength of CEM III cement mortars. The compressive strength of mortar predicted by Power's formula is according to Equation 7.

$$R_c(t) = R_0 \times \left(\frac{0.68 \alpha(t)}{0.32 \alpha(t) + \frac{w}{c}} \right)^n \quad (7)$$

where $R_c(t)$ is Compressive strength of mortar (MPa) after t days of hydration, R_0 is Compressive strength of mortar when the capillary porosity is equal to 0. It is calibrated from the experimental compressive strength measured after 2 days of curing, $\alpha(t)$ is DoH of hydrated cement, $\frac{w}{c}$ is Water to cement mass ratio of mortar and n is Constant depending on the cement type.

Due to the simultaneous hydration of clinker and SCMs [54], the hydration kinetics of multi-composite cement are extremely complex, so the degree of hydration (DoH) of these cements could not be directly determined by TGA like it could with OPC [42, 55, 56]. Despite several methods such as selective dissolution, isothermal calorimetry, chemical shrinkage, and image treatment have been used to determine the DoH of CEM III cement [57], these methods usually require a complex measurement process. Thus, in this study, the DoH of multi-composite cements was determined using the modified TG method. Based on the result found in a previous study [58], the activity coefficient of SF sediment and GBFS was used to convert a certain quantity of mineral additions into an equivalent quantity of Portland pure cement. The activity coefficient of SF sediment and GBFS was determined according to NF EN 206-1 [59]. Therefore, a quantity of CEM III cement could be converted into a quantity of Portland pure cement according to Equation 8:

$$L_{eq} = m_C + K \times m_A \tag{8}$$

where L_{eq} , m_C , m_A are the mass of equivalent binder, mass of cement and mass of mineral addition respectively.

K is the activity coefficient of mineral addition obtained by the compressive strength test performed on the mortar sample with a substitution rate of mineral addition of 25 wt.% according to NF EN 206-1 [59].

As $Ca(OH)_2$ has been consumed by GBFS and SF sediment during cement hydration, the DoH of these cements was determined by measurement of chemically bound water content from the TGA result according to Equation 9.

$$\alpha(t) = \frac{W_b(t)}{W_b(\infty)} \times 100\% \tag{9}$$

where $W_b(t)$ is Chemically bound water content of paste after t days of hydration, $W_b(\infty)$ is Ultimate chemically bound water content corresponding to a complete hydration of equivalent anhydrous cement.

The $W_b(\infty)$ value depends on the mineralogical composition of clinker as well as the type and substitution level of mineral addition [60]. For Portland cement, the $W_b(\infty)$ value can be estimated using the method proposed by NIST (National Institute of Standards and Technology) according to Equation 10 [61].

$$W_n(\infty) = W_{nC_3S}(\infty) \times (\%C_3S) + W_{nC_2S}(\infty) \times (\%C_2S) + W_{nC_3A}(\infty) \times (\%C_3A) + W_{nC_4AF}(\infty) \times (\%C_4AF) + W_{nCaO_{free}}(\infty) \times (\%CaO_{free}) \tag{10}$$

where $W_{nC_3S}(\infty)$, $W_{nC_2S}(\infty)$, $W_{nC_3A}(\infty)$, $W_{nC_4AF}(\infty)$, $W_{nCaO_{free}}(\infty)$ are the ultimate chemically bound water amount of C_3S , C_2S , C_3A , C_4AF and CaO_{free} respectively corresponding to the complete hydration of each phase. $(\%C_3S)$, $(\%C_2S)$, $(\%C_3A)$, $(\%C_4AF)$, $(\%CaO_{free})$ correspond to the content of C_3S , C_2S , C_3A , C_4AF and CaO_{free} respectively.

The activity coefficient of GBFS and SF sediment as well as the ultimate chemically bound water per 1g of each mineralogical phase are given in Table 7.

Table 7. Ultimate chemically bound water per 1g of individual mineralogical phase and activity coefficient of GBFS and SF sediment

Mineralogical phase	Chemically bound water amount per g produced per 1 g of mineralogical phase for a complete hydration
C_3S	0.24
C_2S	0.21
C_3A	0.4
C_4AF	0.37
CaO_{free}	0.33
Activity coefficient of mineral addition	
GBFS	0.9
SF sediment	0.8

Based on the mineralogical composition of CEM III Ref and CEM III SF cements, the ultimate chemically bound water amount per 100 g of equivalent anhydrous cement was calculated using the values given in Table 7, and the result is shown in Table 8.

Table 8. Mineralogical composition and the $W_b(\infty)$ value of both CEM III cements

Composition (wt.%)	CEM III Ref	CEM III SF
C_3S	35.71	35.67
C_2S	9.13	9.12
C_3A	5.45	5.45
C_4AF	5.32	5.31
CaO_{free}	0.93	0.93
Gypsum	5.76	5.86
GBFS	37.7	28.24
SF sediment	-	9.41
Total	100	99.99
$W_b(\infty)$ per 100 g equivalent anhydrous cement	23.97	23.71

However, TGA also usually requires a complex process for preparation and measurement time, especially for samples that are cured long-term. Thus, to save measurement time, a novel approach based on the curve fitting method was applied to determine the DoH of hydrated cement from only a few experimental values. The exponential three-parameter equation proposed by Pane and Hansen [60] was used to establish the DoH curve according to Equation 11:

$$\alpha(t) = \alpha(\infty) \times \exp \left[\left(-\frac{t_c}{t} \right)^a \right] \quad (11)$$

where $\alpha(t)$ is Degree of hydration of cement after t days of curing, $\alpha(\infty)$ is Ultimate degree of hydration of cement, t is Hydration time of cement (days), t_c is Time parameter (days), a is Empirical parameter depending on the type and the substitution rate of supplementary cementitious materials

The DoH of two cement pastes measured by TGA at 2, 15, and 28 days was first plotted using Origin Pro software based on an ordinary least squares regression. Then, the interpolation of the DoH curve was carried out to determine the values $\alpha(\infty)$, t_c and a . Finally, the DoH of CEM III cements at any given time could be easily determined using Equation 8. However, it should be noted that the hydration rate of cement is very fast the first time, so the authors recommend that the TGA should be performed on the cement pastes before 3 days to better fit the DoH curve.

3.2.3. Microstructure of Mortars

The Mercury Intrusion Porosimetry (MIP) method was used to study the microstructure of CEM III cement-based mortars. Mortar samples were cut into small pieces of $1 \times 1 \times 1 \text{ cm}^3$, then immersed in the isopropanol solvent for 3 days to stop the hydration. Samples were stored in a desiccator under vacuum for 7 days to evaporate the isopropanol. The MIP porosity was measured using an Autopore IV device, which has a maximum applicable pressure of 200 MPa and can detect a minimum pore diameter of 6 nm.

4. Results and Discussion

4.1. Hydration Kinetics of Cements

4.1.1. Hydration Heat

The heat flux and the cumulative heat liberated from the hydration of two cement pastes are presented in Figures 5-a and 5-b respectively. The result indicated that SF sediments significantly impacted the hydration kinetics of cement. To assess precisely these changes, the heat evolution curves were separated into three principal periods, in each of which the influence of SF sediment could be more clearly observed.

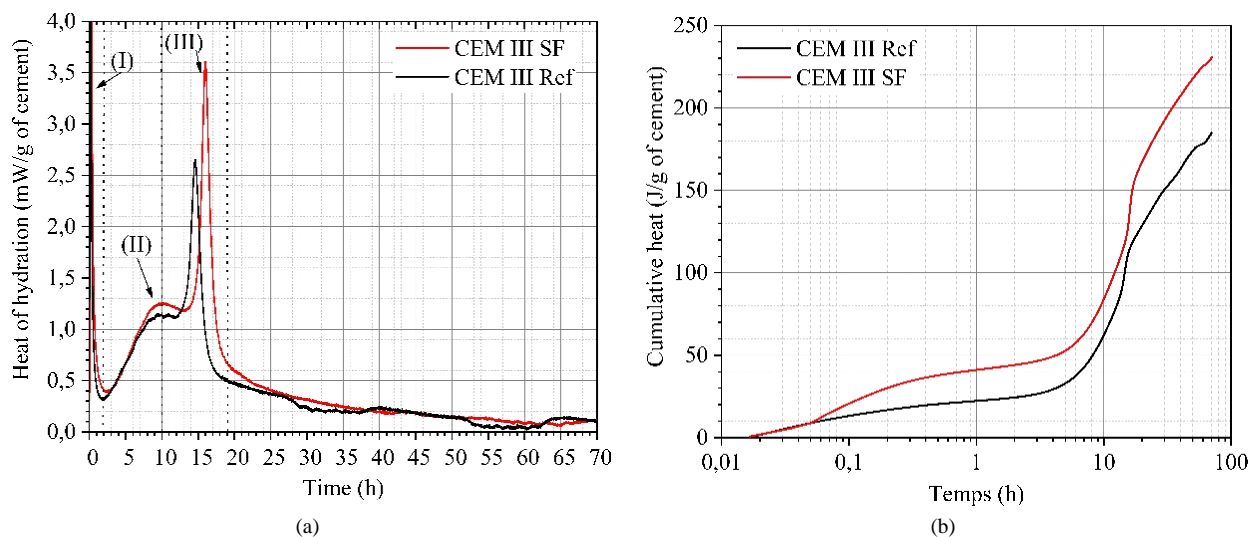


Figure 5. (a) Rate of heat evolution of both hydrated cement pastes ($W/C = 0.5$), (b) Cumulative heat of both hydrated cement pastes ($W/C = 0.5$) measured by isothermal conduction calorimetry analysis

The potential influences of SF sediment on cement hydration can be indicated as follows:

- **Period (I):** The heat released in this period can come from the various possible reactions, including the hydration of CaO_{free} , gypsum, and the C_3A phase [16]. Thus, the potential modification in this stage relates principally to the change in the initial hydration rate of the C_3A phase. An increase in the magnitude of the first peak of CEM III SF cement was observed. The length of the dormant stage of CEM III SF cement was also longer than that of CEM III Ref cement. This delay may be due to a higher BET-specific surface area of CEM III SF cement compared with CEM III Ref as reported in a previous study [62].

- **Period (II):** In this period, the heat liberated generally relates to the hydration of the C_3S phase. It can be seen that SF sediment addition increased the magnitude of the second peak of CEM III SF cement compared to the reference. This result may be due to a higher BET-specific surface area of SF sediment compared to GBFS, resulting in an acceleration of C_3S hydration rate. In addition, $CaCO_3$ in SF sediment accelerated the hydration rate of C_3S as mentioned in previous studies [4, 63, 64].
- **Period (III):** During this time, the heat generated usually links the conversion of ettringite phase (AFt) into mono-sulfoaluminate phase (AFm), the secondary formation of AFt, the hydration onset of C_4AF , or the hydration of GBFS in the case of blast furnace slag cement [16]. The change in magnitude of the peak in this period was much more evident than in periods (I) and (II). A significant increase in the hydration heat of CEM III SF cement could confirm that SF sediment impacted the hydration rate of C_3A more than GBFS. This result is supported by the findings of a previous study [63], which showed that the intensity of this peak increased by nearly 50% in the case of white cement containing limestone when compared to pure white cement.

The cumulative hydration heat of two cement pastes is shown in Figure 5-b. As indicated above, the SF sediment substitution accelerated the clinker phase hydration, leading to a significant increase in the cumulative hydration heat of CEM III SF cement compared with the reference. Indeed, after 72 hours of hydration, the cumulative hydration heat of CEM III SF cement was 230 J/g, while CEM III Ref cement was only 185 J/g.

4.1.2. Chemically Bound Water and $Ca(OH)_2$ Content

The chemically bound water content of CEM III Ref and CEM III SF pastes over time, normalized per 100 g of anhydrous cement is shown in Figure 6.

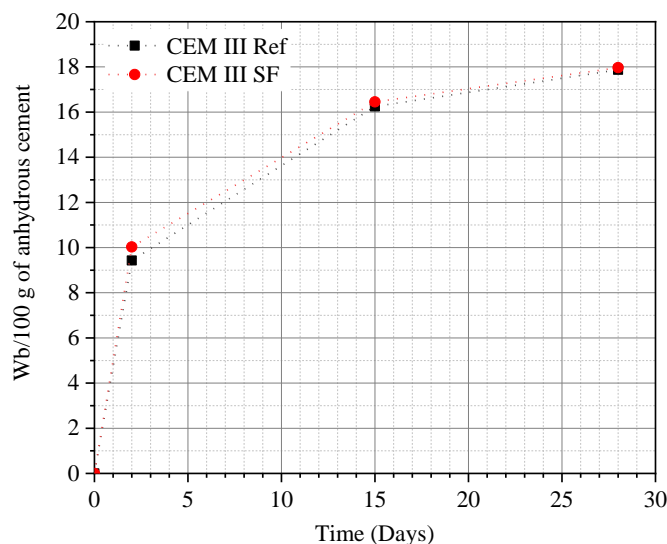


Figure 6. Chemically bound water content of CEM III Ref and CEM III SF pastes as a function of time normalized per 100 g of anhydrous cement

Chemically bound water content increased with time for all two investigated binders. However, it can be seen that the chemically bound water content of CEM III SF cement was always higher than that of CEM III Ref cement, especially at early ages (2 days). This was in accordance with the result obtained by isothermal conduction calorimetry analysis, which also indicated an accelerating effect of SF sediment on cement hydration. In fact, since the SF sediment has a higher BET-specific surface area than the GBFS, this could improve the nucleation sites for the hydration products of the clinker phases, leading to more hydration products in the CEM III SF than in the CEM III Ref cement at early ages. This is similar to the results obtained in previous studies [65, 66] which also indicated that the changes in hydration kinetics are dominated by the filler effect in the first days.

An increase in the chemically bound water amount of the CEM III SF cement compared to the CEM III Ref cement at later ages could be attributed to a higher reactivity of the pozzolanic reaction of the SF sediment-GBFS system than the GBFS alone. Since the pozzolanic material reacts with the $Ca(OH)_2$ to form the calcium silicate hydrate [67], the pozzolanic reactivity of the GBFS or the SF sediment-GBFS system could be investigated by measuring the $Ca(OH)_2$ content. From the TGA result, the $Ca(OH)_2$ content of two cement pastes normalized per 100 g of anhydrous cement is shown in Figure 7. As expected, the $Ca(OH)_2$ content of CEM III SF cement was much higher than that of CEM III Ref cements at early ages. Since clinker content in the two cements is nearly similar (Table 4), an increase in $Ca(OH)_2$ content of CEM III SF cement confirmed that clinker hydration was accelerated in the presence of SF sediment, leading

to more $\text{Ca}(\text{OH})_2$ formation. Additionally, it can be seen that for the two cement pastes, after 15 days of hydration, the $\text{Ca}(\text{OH})_2$ content decreased, whereas the chemically bound water content increased. This demonstrated clearly that $\text{Ca}(\text{OH})_2$ produced by clinker reactions was consumed by the pozzolanic reaction of GBFS and SF sediment. A similar result was also reported in a previous study [68] which also indicated that the $\text{Ca}(\text{OH})_2$ amount increased in the first days, and decreased in the long-term.

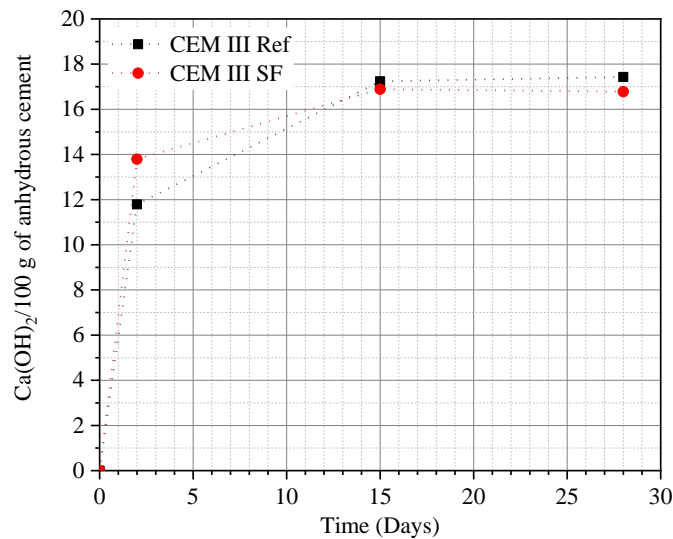


Figure 7. $\text{Ca}(\text{OH})_2$ content of CEM III Ref and CEM III SF pastes as a function of time normalized per 100 g of anhydrous cement

Comparing $\text{Ca}(\text{OH})_2$ content and chemically bound water content between CEM III Ref and CEM III SF pastes indicated that after 15 days of hydration, the $\text{Ca}(\text{OH})_2$ content consumed by the SF sediment-GBFS system was higher than that consumed by GBFS alone. This result suggested that the pozzolanic reactivity of the SF sediment-BGFS system was higher than that of BGFS alone.

4.1.3. Hydrates Assemblages of Hydrated Cements

The hydration products formed in both cement pastes after 28 days of hydration are presented in Figure 8.

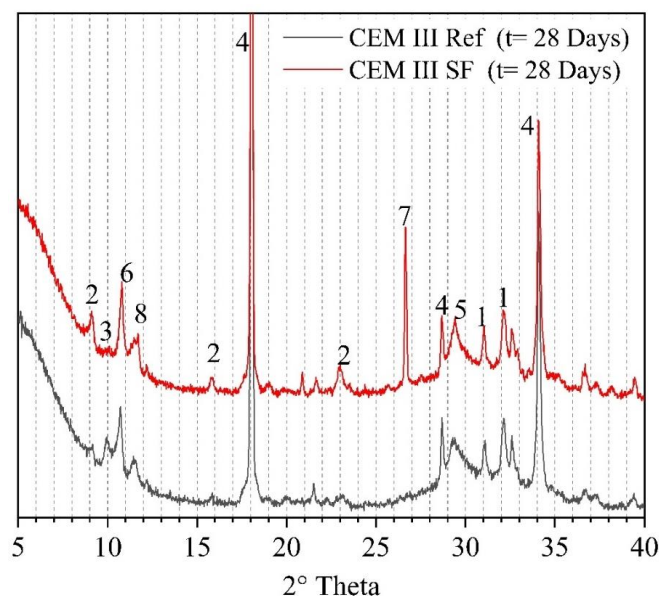


Figure 8. XRD patterns of hydrated cements after 28 days of curing. (1): $\text{C}_3\text{S} + \text{C}_2\text{S}$, (2): Ettringite (AFt), (3): Mono-sulfoaluminate (AFm), (4): Portlandite (CH), (5): C-S-H/C-A-S-H + CaCO_3 , (6): Hemi-carboaluminate, (7) Quartz, (8) Hydrotalcite-like (HT).

In general, most hydration products produced from CEM III Ref and CEM III SF cement hydration were similar. The hydration products identified were ettringite, mono-sulfoaluminate, $\text{Ca}(\text{OH})_2$, hemi-carboaluminate, hydrotalcite-

like (Ht) and C-S-H/C-A-S-H and CaCO_3 . These hydrates were also typical hydrates produced during the hydration of the slag-blended cement systems, as indicated in previous studies [7, 69, 70].

However, the peaks of stratlingite (at 7.1° and 14.2°) [71] were not observed in the XRD patterns of both cement pastes after 28 days of hydration. This observation was also in accordance with the result indicated in a previous study [54, 69] that used thermodynamic modeling to predict the formation of hydration products as a function of slag rate in the slag-blended cement. The modeling result indicated that the formation of stratlingite occurred when the slag amount was greater than 65%.

Additionally, it can be seen that after 28 days of hydration, the magnitude of $\text{Ca}(\text{OH})_2$ peaks at 18° , 29.8° and 34° [40, 72] of CEM III SF paste was slightly less than that of CEM III Ref paste. This was also similar to the result obtained by the TG analysis shown in Figure 7.

The hydrotacite-like (Ht) phase [73, 74] formed from the reaction between GBFS and $\text{Ca}(\text{OH})_2$ as described in Eq (1) was also identified for two hydrated cements, whereas the C-S-H/C-A-S-H phase is generally indistinguishable by XRD analysis due to its amorphous nature. However, SF sediment substitution also led to some changes in hydration products when compared to the CEM III Ref cement, as follows:

- Compared to the reference, the ettringite (AFt) peaks at 9.1° , 15.9° , and 23.1° [75] were much stronger in CEM III SF paste, whereas the mono-sulfoaluminate (AFm) peak at 9.9° [75] was much weaker. This is very likely due to a higher CaCO_3 amount of SF sediment than BGFS, and this has decreased the dissolution of the AFt phase into the amorphous mono-sulfoaluminate phase [64, 76]. The formation of hemi- or mono-carboaluminates instead of mono-sulfoaluminate led to a greater available of sulfate to form more ettringite [77]. Thus, this explained how, despite the similar sulfate content of the two cements, the AFt content of CEM III SF paste was higher than the reference.
- The hemi-carboaluminate content of CEM III SF paste was slightly higher than that of CEM III Ref paste. Since the C_3A amount of both cements is similar (Table 8), an increase in hemi-carboaluminate content for CEM III SF paste compared with CEM III Ref paste was essentially due to a higher CaCO_3 amount of CEM III SF cement than CEM III Ref cement. Indeed, the formation of hemi- and mono-carboaluminates in the blended cement often increases with an increase in the CaCO_3 amount [78]. In addition, a quartz peak (at 26.6°) was identified in the XRD patterns of CEM III SF paste only. This was consistent with results indicated in previous studies [33] which indicated the peak of quartz in the XRD patterns of blended cement containing the sediment. This indicated that quartz in SF sediment did not participate in cement hydration, and the influence on the chemical composition of hydrates was investigated by SEM-EDS analysis.

Beside the investigation based on the XRD analysis result, derivative thermogravimetry (DTG) analysis was performed to provide a more in-depth description of the content of hydrates formed, particularly in the case of C-H-H gels. Figure 9 shows the DTG curves of both cement pastes after 28 days of curing.

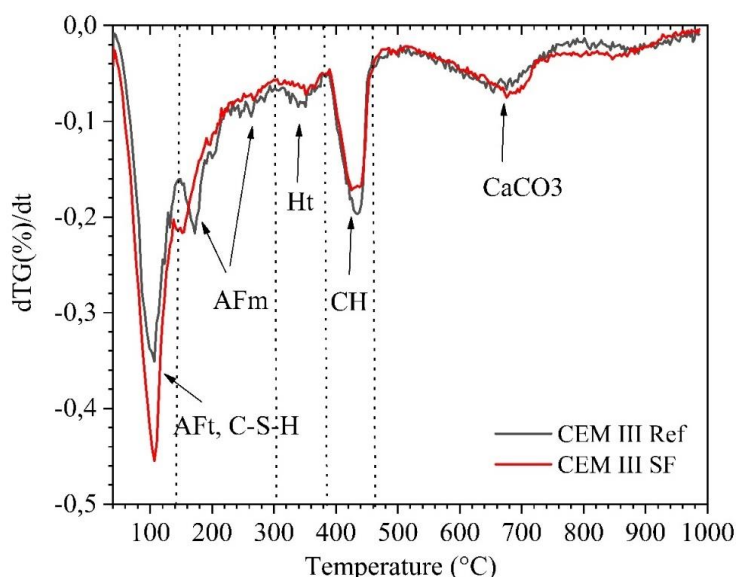


Figure 9. DTG curve of CEM III Ref and CEM III SF cement pastes after 28 days of curing

The first peak of the DTG curve around 110°C is principally related to the dehydration of the AFt and C-S-H phases [79, 80]. The dehydration of the AFm phase occurs in the temperature range between 140°C and 300°C , with a main peak at 180°C . The third main peak at 360°C corresponds to the decomposition of hydrotalcite-like [81], while the dehydration of $\text{Ca}(\text{OH})_2$ occurs in the temperature range between 400°C and 460°C [82]. It can be seen that after 28

days of hydration, SF sediment incorporation resulted in a significant increase in the intensity of the C-S-H/AFt peak and a decrease in the magnitude of the $\text{Ca}(\text{OH})_2$ peak. This also suggested that the C-S-H content formed from CEM III SF cement hydration could be higher than that of CEM III Ref cement.

4.1.4. Chemical Composition of C-S-H Gels

The chemical composition of C-S-H gels, including the inner C-S-H and the outer C-S-H, formed in CEM III Ref and CEM III SF pastes at 28 days determined by SEM-EDS analysis is shown in Figures 10-a and 10-b respectively, as the two-dimensional scatter plots of atomic ratios (Si:Ca for the X-axis, Al:Ca for the Y-axis).

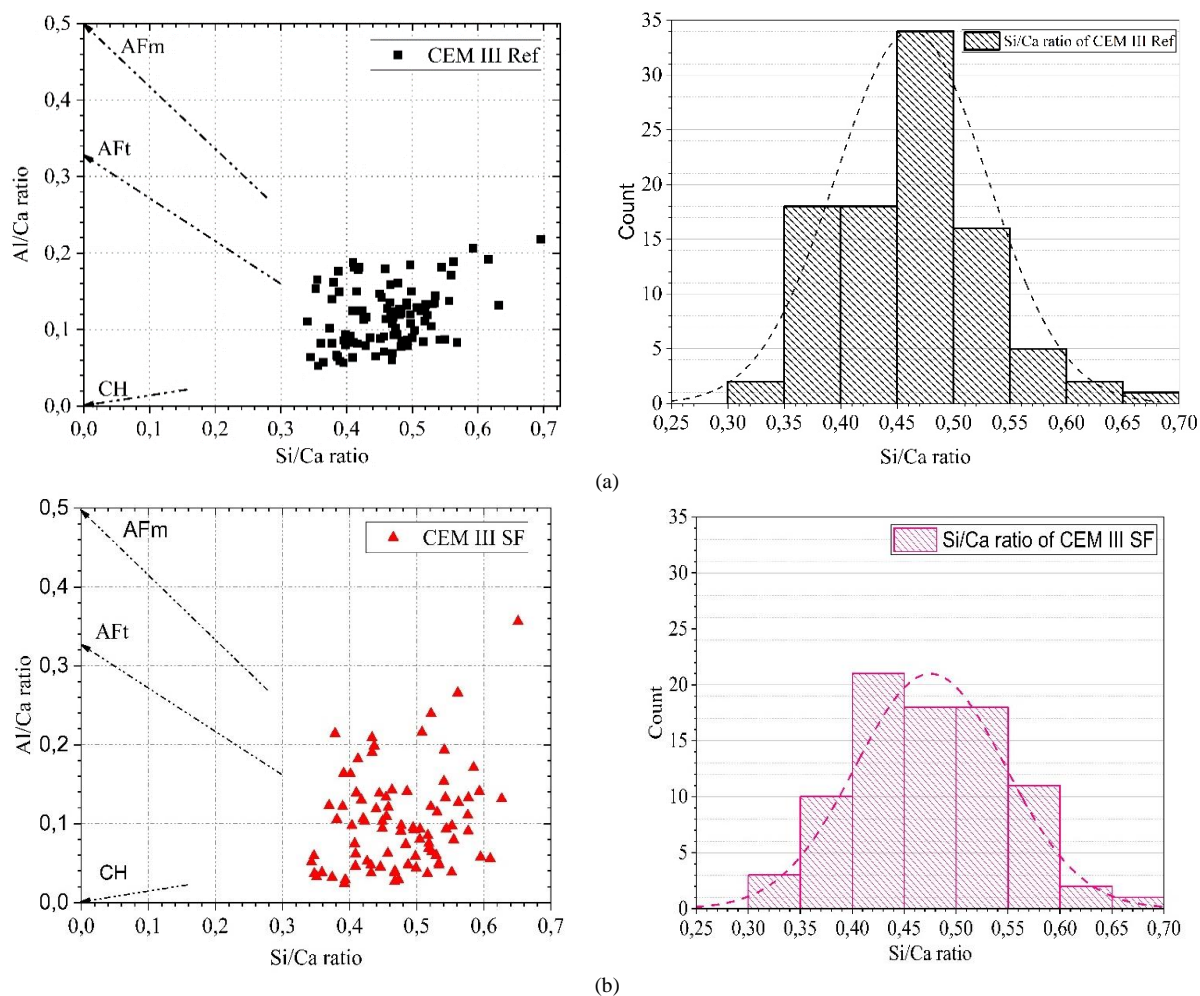


Figure 10. (a) Scatter plot of C-S-H gels formed in the CEM III Ref, (b) Scatter plot of C-S-H gels formed in the CEM III SF paste after 28 days of hydration

The result showed that the chemical composition of C-S-H gels produced from the hydration of the two cements was not too different. The Si/Ca ratio range was between 0.35 and 0.55 corresponding to the Ca/Si ratio range between 1.81 and 2.86, respectively. These ratios were also similar to those reported in a previous study [83] with an average Si/Ca ratio of 0.65 ± 0.02 . However it can be seen that the Ca/Si ratio range obtained in this study for both cement pastes was higher than the value of 1.60 reported in the previous studies [16, 84]. This difference can be due to numerous reasons, such as the chemical composition of the mineral admixture, curing time, change in the voltage of the electron microprobe analysis, presence of foreign elements coming from the interstitial clinker phases, change in the water-to-cement ratio [85], or interaction of the volume of hydrates in the SEM-EDS analysis [86]. Thus, the result can contain signals from the intermixing of C-S-H with $\text{Ca}(\text{OH})_2$ or C-S-H with ettringite.

In addition, this result also indicated that the mean Ca/Si ratio of C-S-H gels of CEM III SF paste was slightly higher than that of CEM III Ref paste, whereas the CaO/SiO_2 ratio obtained by XRF analysis was much lower, with a ratio of 2.09 for CEM III SF and 2.33 for CEM III Ref respectively. As indicated in XRD patterns of CEM III SF cement pastes at 28 days, the presence of quartz in SF sediment reduced the soluble amount of SiO_2 soluble for reaction with $\text{Ca}(\text{OH})_2$ to form C-S-H gels, leading to an increase in the Ca/Si ratio of C-S-H gels of CEM III SF paste compared with the CEM III Ref paste.

In addition, the uptake of Al^{3+} ions in C-S-H gels was detected in both cement pastes, with a mean Al/Si ratio of 0.266 for CEM III Ref and 0.237 for CEM III SF pastes, respectively. These ratios are significantly higher than the value

obtained for Portland cement, which was in the range of 0.05-0.10 [87]. The incorporation of Mg^{2+} ions was also identified in C-S-H gels in different amounts depending on the Ca/Si ratio, as shown in Figure 11. The result also indicated that the MgO/Al_2O_3 ratio decreased with an increase in the CaO/SiO₂ ratio of C-S-H gels. This appeared to be contrary to the results found in the previous studies [18, 88], which indicated that magnesium was incorporated with a very slight content in C-S-H gels. However, it should be noted that intermixing of hydrates can influence the analysis result.

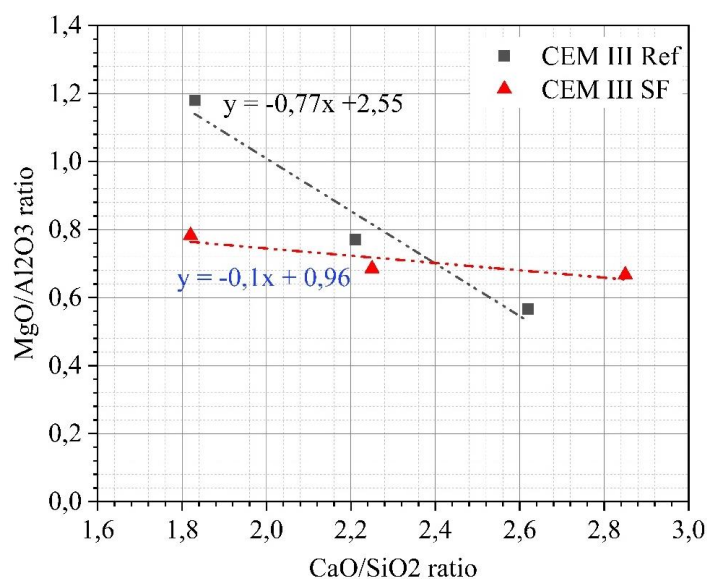


Figure 11. MgO/Al_2O_3 versus CaO/SiO_2 ratio in the C-S-H gels of both cement pastes measured by SEM-EDS analysis

4.2. Compressive Strength and Microstructure

4.2.1. Compressive Strength

The compressive strengths of CEM III Ref and CEM III SF mortars are presented in Figure 12. The CEM Ref cement had compressive strengths of 14.97 MPa at 2 days, 29.58 MPa at 7 days, and 46.96 MPa at 28 days, while these strengths of CEM III SF cement were 19.68 MPa, 38.11 MPa, and 48.98 MPa, respectively. This result indicated that SF sediment substitution significantly improved the strength of mortar compared with the reference mortar, especially at early ages. For instance, the compressive strength of CEM III SF mortar is 33% higher after 2 days and 4.5% higher after 28 days compared to that of CEM III Ref mortar. The improvement of strengths of CEM III SF mortar at early ages was principally due to the accelerating effect of SF sediment on the cement hydration as indicated by the isothermal conduction calorimetry and TG analysis. The increase in the strength of CEM III SF mortar at long-term could be attributed to the higher pozzolanic reactivity of the SF sediment-GBFS system compared to the GBFS alone. This led to the formation of more calcium silicate hydrate, which refined the pore structure and improved the compressive strength of mortar [89].

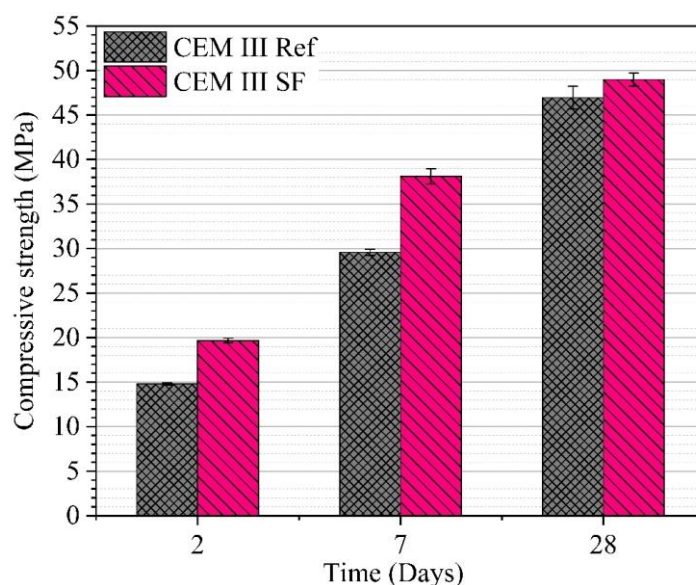


Figure 12. Compressive strength of CEM III Ref and CEM III SF mortars as a function of time

After 28 days, the compressive strength of two standard mortars was higher at 42.5 MPa, so both cements can be classified as CEM III 42.5 type according to NF EN 197-1 [20].

4.2.2. Compressive Strength Mortars Predicted by Novel Approach

The DoH of two equivalent cements measured by TGA is presented in Figure 13.

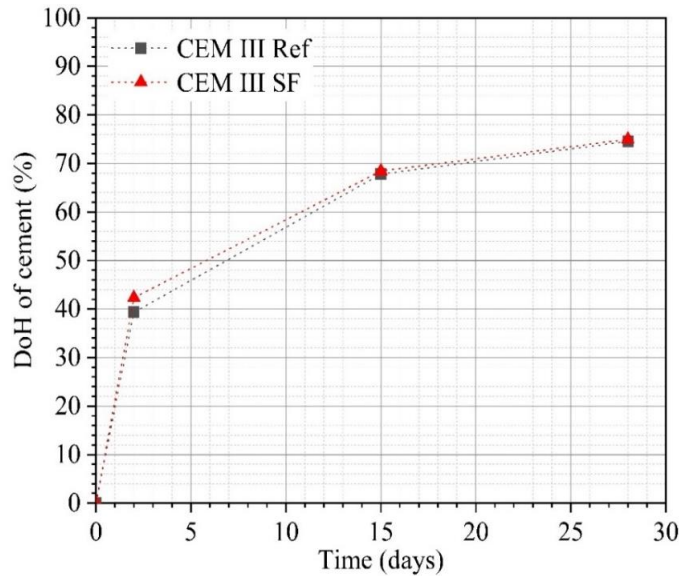


Figure 13. DoH of CEM III Ref and CEM III SF cements measured by TGA

As expected, the DoH of CEM III SF cement was always higher than that of the reference, especially at early ages. The DoH of CEM III Ref cement reached 38.8% at 2 days and 74.6% at 28 days, while for CEM III SF cement, these values were 41.5% at 2 days and 75.6% at 28 days, respectively. Compared to the DoH of ordinary Portland cement made with the same water-to-cement ratio (W/C = 0.5) obtained in the previous studies [41, 42], the DoH of two CEM III cements in this study was much lower, especially at early ages (DoH = 56.28% for OPC at 2 days) [41, 42, 56]. This was due to the fact that SCMs reactivity such as GBFS or SF sediment is much lower than clinker [7]. Thus, the DoH of two equivalent cements obtained in this study using the coefficient of activity was reasonable.

From the experimental results of the DoH, Figures 14-a and 14-b shows the DoH curve obtained from the curve fitting method for CEM III Ref and CEM III SF cements respectively. It can be seen that there is a good agreement between the DoH values obtained by the curve fitting method and the experiment for the two cement pastes.

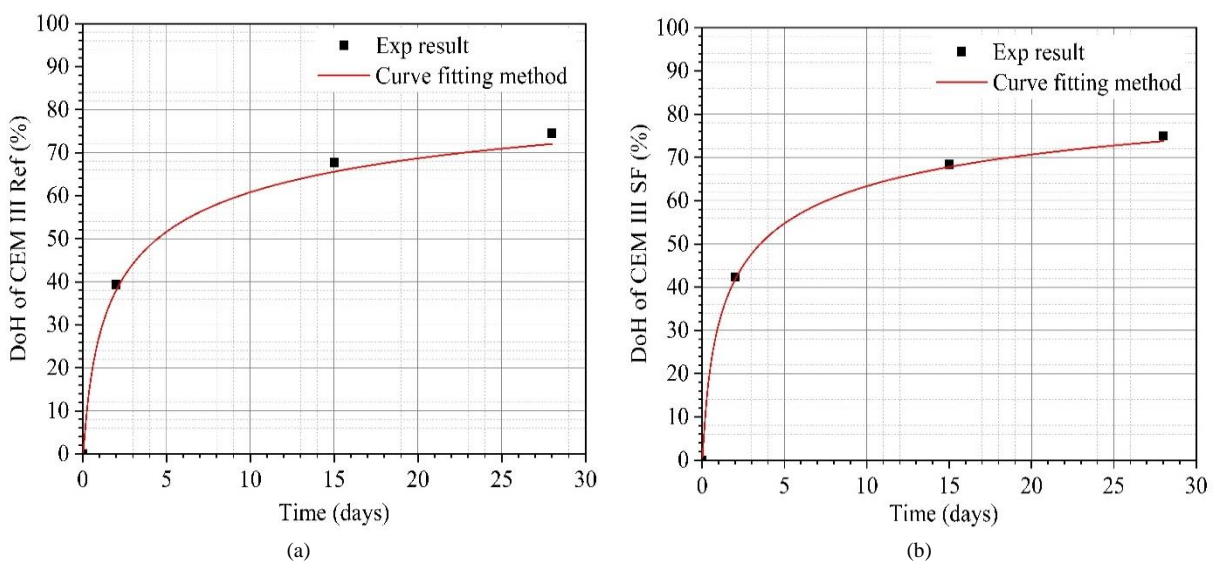


Figure 14. DoH curve obtained from the experimental measurement (TGA analysis) and the curve fitting method. (a) CEM III Ref, (b) CEM III SF

Based on the DoH curve obtained above, Figures 15-a and 15-b present simultaneously the strengths predicted by the model according to Equation 4 and experimental data for CEM III Ref and CEM III SF mortars, respectively. A

good agreement between the experimental result and the model result was observed for the two mortars. For instance, for the compressive strength of mortars after 7 days, although the DoH of both cement pastes was not measured in the time period, this model could predict the relatively accurate strength of both mortars compared to the experimental results. This also meant that the DoH of both cement pastes could be accurately predicted using the curve fitting method. Overall, this result demonstrated that this novel approach can be used as a reliable tool for the prediction of the compressive strength of multi-composite cement-based mortars.

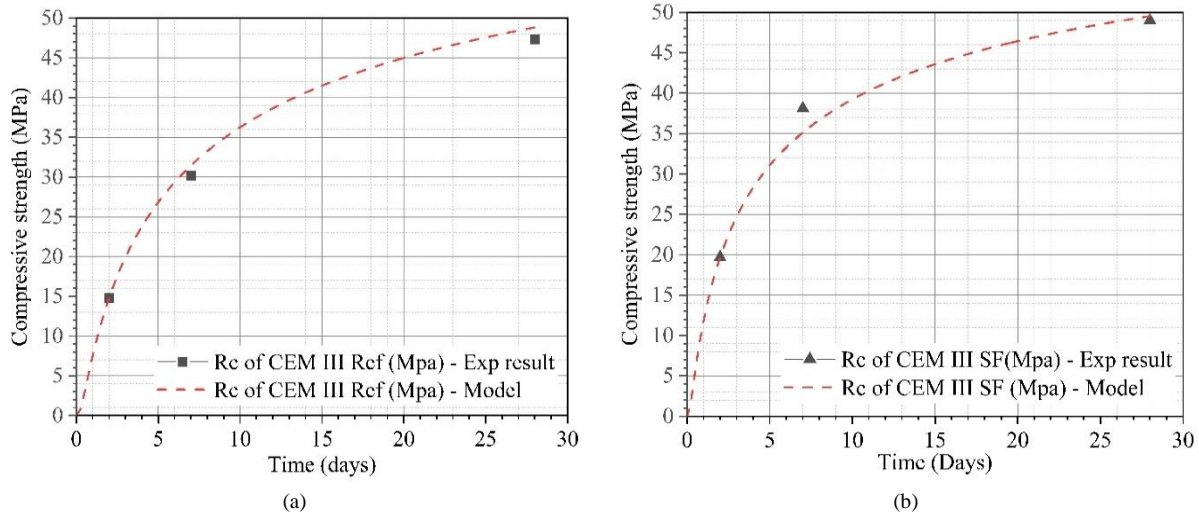


Figure 15. Compressive strength obtained from the experimental measurement and prediction model (a) CEM III Ref mortar, (b) CEM III SF mortar

4.2.3. Microstructure Development

The porosity of both mortars measured by the MIP method at 2 and 28 days of hydration is shown in Figure 16-a. By comparison with the reference mortar, it can be seen that the SF sediment incorporation significantly decreased the porosity of CEM III SF mortars by 16.33% at 2 days, and by 12.40% at 28 days, respectively. This confirmed our findings on the compressive strength results already shown.

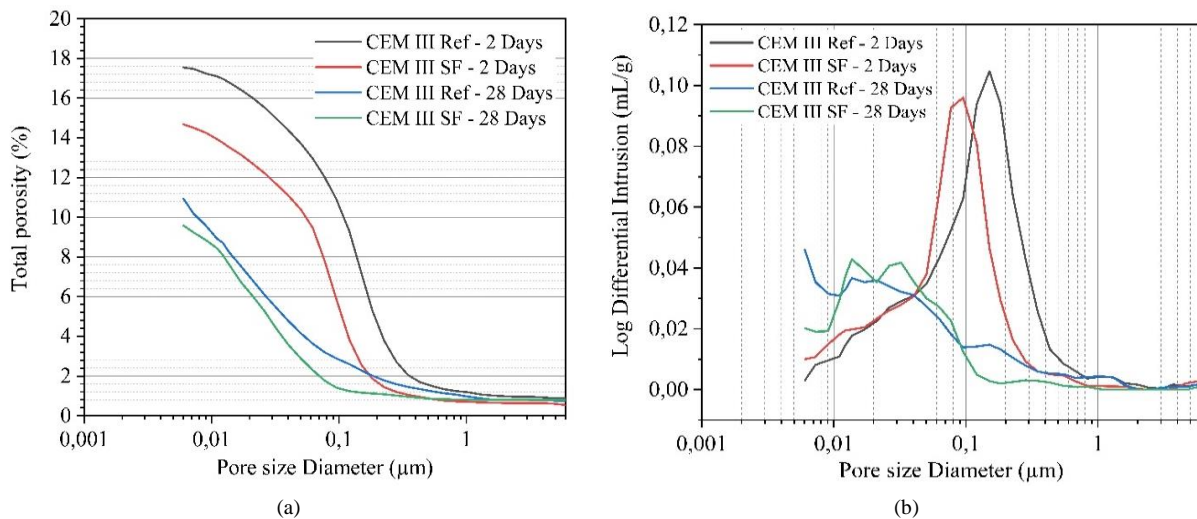


Figure 16. (a) Total porosity of mortars measured by MIP technique, (b) Pore size distribution of mortars measured by MIP after 2 and 28 days of hydration

Since the clinker amounts of both cements are similar, the porosity reduction of CEM III SF mortar could be due to the following reasons:

- (i) The SF sediment substitution accelerated cement hydration, leading to an increase in solid volume and infilling the pore as demonstrated in previous studies [90, 91].
- (ii) A higher pozzolanic reactivity of the SF sediment-GBFS system compared to the GBFS alone could also contribute to the enhancement of CEM III SF microstructure [92, 93]. Indeed, previous studies [76, 84] indicated that the consumption of $\text{Ca}(\text{OH})_2$ by the pozzolanic reaction could lead to densification of the microstructure and a decrease in the pore connectivity.

- (iii) The stabilization of ettringite against the conversion to AFm phase in CEM III SF as indicated in the XRD pattern also contributed to the decrease in the porosity because this conversion could lead to a less efficient filling of pores, which increased the total porosity [93].

To investigate the effects of SF sediment substitution on the transport properties of mortar, the pore size distribution (PSD) of two mortars at 2 and 28 days of hydration presented in Figure 16-b was studied. The critical pore diameter (CPD) is defined as the inflexion point of the cumulative curve or the maximum of the capillary peak of the derivative curve [76]. Beside the decrease in the total porosity, the SF sediment substitution also reduced the CPD of CEM III SF mortar compared to the reference. For instance, after 2 days, the CPD of mortar decreased from 0.06 μm for CEM III Ref mortar to 0.04 μm for CEM III SF mortar. The MIP measurement result also confirmed that a SF sediment substitution rate of 25%.wt significantly improved the microstructure of mortar, and this could enhance the durability properties of mortar or concrete, as reported in a previous study [95].

5. Conclusions

The objectives of this study were to investigate the impacts of GBFS replacement by flash-calcined sediment (SF sediment) on the hydration kinetics and mechanical-microstructural properties of CEM III cement. In addition, a novel approach based on a combination of the curve fitting method and Power's empirical relation was established to predict the compressive strength of multi-composite cement-based mortars. From the results obtained in this study, the following conclusion can be drawn:

1) Hydration kinetics:

- The SF sediment substitution with a rate of 25%.wt significantly improved the hydration of CEM III cement compared with the reference cement, especially at early ages. A higher BET-specific surface area of SF sediment compared to GBFS provided more available surface for hydrate precipitation, leading to an increase in the CEM III SF cement hydration rate. In addition, CaCO_3 in SF sediment also has positive impacts on the hydration of the C_3A phase and the stabilization of ettringite against the conversion to mono-sulfoaluminate (AFm), improving the microstructure of CEM III SF mortar.
- The TGA result also indicated that the SF sediment-GBFS system was more reactive than GBFS alone, and this led to the formation of more calcium silicate hydrate in the CEM III SF cement.
- The SF sediment substitution did not significantly alter the chemical composition of calcium silicate hydrate. The Ca/Si ratio range of C-S-H gels was from 1.82 to 2.84 for both cement paste samples. The quartz (SiO_2) in SF sediment reduced the soluble amount of $\text{SiO}_{2\text{soluble}}$ in CEM III SF paste, leading to an increase in the Ca/Si mean ratio of C-S-H gels in CEM III SF compared with the reference. Mg^{2+} and Al^{3+} ion incorporation was also identified in C-S-H gels with different ratios, depending on the Ca/Si ratio. The Mg/Al ratio decreased with an increase in the Ca/Si ratio of C-S-H gels.

2) Mechanical-microstructural properties:

- The SF sediment substitution significantly improved the compressive strength of CEM III SF mortar compared to the reference mortar with an increase of 33% after 2 days and 16.33% after 28 days respectively. The microstructural analysis performed on the mortar samples also confirmed that the SF substitution significantly reduced the porosity and the critical pore diameter of CEM III SF mortar compared to the reference.
- A novel approach based on a combination of the curve fitting method and Power's empirical relation could accurately predict the strength development of multi-composite cement-based mortars over time. The advantage of this model is that it allows one to predict the compressive strength of multi-composite cement-based mortars without needing to know the compressive strength of a reference mortar, unlike two of the most commonly used models, the Bolomey model and the Feret model.

Overall, according to the results obtained from this study, it can be concluded that the SF sediment could be used as a replacement for GBFS in the CEM III production with positive impacts on hydration and the development of mechanical-microstructural properties. This solution is promising for developing an eco-friendly binder in the cement and concrete sectors.

6. Declarations

6.1. Author Contributions

Conceptualization, M.B., D.C.C., M.A., N.A., and J.N.; methodology, M.B., D.C.C., M.A., N.A., N.A., and J.N.; validation, M.B., M.A., M.A., N.A., and J.N.; investigation, D.C.C.; writing—original draft preparation, D.C.C.; writing—review and editing, M.B., M.A., N.A., and J.N.; visualization, D.C.C.; supervision, M.B., M.A., N.A., and J.N. All authors have read and agreed to the published version of the manuscript.

6.2. Data Availability Statement

The data presented in this study are available on request from the corresponding author.

6.3. Funding and Acknowledgments

The authors wish to acknowledge the SEDICIM project and the FEDER funds.

6.4. Conflicts of Interest

The authors declare no conflict of interest.

7. References

- [1] Barcelo, L., Kline, J., Walenta, G., & Gartner, E. (2014). Cement and carbon emissions. *Materials and Structures / Materiaux et Constructions*, 47(6), 1055–1065. doi:10.1617/s11527-013-0114-5.
- [2] Matschei, T., Lothenbach, B., & Glasser, F. P. (2007). The role of calcium carbonate in cement hydration. *Cement and Concrete Research*, 37(4), 551–558. doi:10.1016/j.cemconres.2006.10.013.
- [3] Bentz, D. P., Ferraris, C. F., Jones, S. Z., Lootens, D., & Zunino, F. (2017). Limestone and silica powder replacements for cement: Early-age performance. *Cement and Concrete Composites*, 78, 43–56. doi:10.1016/j.cemconcomp.2017.01.001.
- [4] Bentz, D. P., Jones, S. Z., & Lootens, D. (2016). Minimizing Paste Content in Concrete Using Limestone Powders - Demonstration Mixtures. National Institute of Standards and Technology. doi:10.6028/nist.tn.1906.
- [5] De Weerd, K., Haha, M. Ben, Le Saout, G., Kjellsen, K. O., Justnes, H., & Lothenbach, B. (2011). Hydration mechanisms of ternary Portland cements containing limestone powder and fly ash. *Cement and Concrete Research*, 41(3), 279–291. doi:10.1016/j.cemconres.2010.11.014.
- [6] Proske, T., Rezvani, M., Palm, S., Müller, C., & Graubner, C. A. (2018). Concretes made of efficient multi-composite cements with slag and limestone. *Cement and Concrete Composites*, 89, 107–119. doi:10.1016/j.cemconcomp.2018.02.012.
- [7] Zajac, M., Skocek, J., Adu-Amankwah, S., Black, L., & Ben Haha, M. (2018). Impact of microstructure on the performance of composite cements: Why higher total porosity can result in higher strength. *Cement and Concrete Composites*, 90, 178–192. doi:10.1016/j.cemconcomp.2018.03.023.
- [8] Joshi, R. C., & Lohita, R. P. (1997). *Fly ash in concrete: production, properties and uses (Vol. 2)*. CRC Press, Boca Raton, United States.
- [9] Boddy, A. M., Hooton, R. D., & Thomas, M. D. A. (2003). The effect of the silica content of silica fume on its ability to control alkali-silica reaction. *Cement and Concrete Research*, 33(8), 1263–1268. doi:10.1016/S0008-8846(03)00058-9.
- [10] Teklay, A., Yin, C., Rosendahl, L., & Kjøhler, L. L. (2015). Experimental and modeling study of flash calcination of kaolinite rich clay particles in a gas suspension calciner. *Applied Clay Science*, 103, 10–19. doi:10.1016/j.clay.2014.11.003.
- [11] Yu, C., Sun, W., & Scrivener, K. (2015). Degradation mechanism of slag blended mortars immersed in sodium sulfate solution. *Cement and Concrete Research*, 72, 37–47. doi:10.1016/j.cemconres.2015.02.015.
- [12] Berthomier, M., Lors, C., Damidot, D., De Larrard, T., Guérandel, C., & Bertron, A. (2021). Leaching of CEM III paste by demineralised or mineralised water at pH 7 in relation with aluminium release in drinking water network. *Cement and Concrete Research*, 143. doi:10.1016/j.cemconres.2021.106399.
- [13] Cyr, M., Lawrence, P., & Ringot, E. (2005). Mineral admixtures in mortars: Quantification of the physical effects of inert materials on short-term hydration. *Cement and Concrete Research*, 35(4), 719–730. doi:10.1016/j.cemconres.2004.05.030.
- [14] Moranville-Regourd, M., & Kamali-Bernard, S. (2019). *Cements Made From Blastfurnace Slag*. *Lea's Chemistry of Cement and Concrete*, 469–507, Butterworth-Heinemann, Oxford, United Kingdom. doi:10.1016/b978-0-08-100773-0.00010-1.
- [15] Yüksel, I., Siddique, R., Khatib, J.M. (2008). Effect of GGBFS and GSS on the properties of mortar. In *Proceedings of the Excellence in Concrete Construction through Innovation*, 9–10 September 2008, Kingston University, London, United Kingdom.
- [16] Richardson, I. G., Wilding, C. R., & Dickson, M. J. (1989). The hydration of blastfurnace slag cements. *Advances in Cement Research*, 2(8), 147–157. doi:10.1680/adcr.1989.2.8.147.
- [17] Sowoidnich, T., Damidot, D., Ludwig, H.-M., Germroth, J., Rosenberg, R., & Cölfen, H. (2023). The nucleation of C–S–H via prenucleation clusters. *The Journal of Chemical Physics*, 158, 114309. doi:10.1063/5.0141255.
- [18] Richardson, J. M., Biernacki, J. J., Stutzman, P. E., & Bentz, D. P. (2002). Stoichiometry of slag hydration with calcium hydroxide. *Journal of the American Ceramic Society*, 85(4), 947–953. doi:10.1111/j.1151-2916.2002.tb00197.x.
- [19] Daube, J., & Bakker, R. (1986). *Portland blast-furnace slag cement: a review*. *Blended Cements*. ASTM International, Pennsylvania, United States. doi:10.1520/STP36388S.

- [20] NF EN 197-1. (2000). Cement - Part 1: composition, specifications and conformity criteria for common cements. Association Française de Normalisation (AFNOR), Saint-Denis Cedex, France. (In French).
- [21] Scrivener, K. L., John, V. M., & Gartner, E. M. (2018). Eco-efficient cements: Potential economically viable solutions for a low-CO₂ cement-based materials industry. *Cement and Concrete Research*, 114, 2–26. doi:10.1016/j.cemconres.2018.03.015.
- [22] Van Bunderen, C., Benboudjema, F., Snellings, R., Vandewalle, L., & Cizer, Ö. (2021). Experimental analysis and modelling of mechanical properties and shrinkage of concrete recycling flash calcined dredging sediments. *Cement and Concrete Composites*, 115. doi:10.1016/j.cemconcomp.2020.103787.
- [23] Faure, A., Coudray, C., Anger, B., Moulin, I., Colina, H., Izoret, L., Théry, F., & Smith, A. (2019). Beneficial reuse of dam fine sediments as clinker raw material. *Construction and Building Materials*, 218, 365–384. doi:10.1016/j.conbuildmat.2019.05.047.
- [24] Chu, D. C., Amar, M., Kleib, J., Benzerzour, M., Betrancourt, D., Abriak, N. E., & Nadah, J. (2022). The Pozzolanic Activity of Sediments Treated by the Flash Calcination Method. *Waste and Biomass Valorization*, 13(12), 4963–4982. doi:10.1007/s12649-022-01789-8.
- [25] Banfill, P. F. G., & Saunders, D. C. (1986). The relationship between the sorption of organic compounds on cement and the retardation of hydration. *Cement and Concrete Research*, 16(3), 399–410. doi:10.1016/0008-8846(86)90116-X.
- [26] Venda Oliveira, P. J. da, Vieira, A. F. V., & Correia, A. A. S. (2017). Effect of organic matter in soft soils on the effectiveness of preloading for foundations. *Proceedings of the Institution of Civil Engineers - Geotechnical Engineering*, 170(4), 305–311. doi:10.1680/jgeen.16.00082.
- [27] Yang, Y., Wu, S., & Huang, X. (2021). Experimental Study on the Effect of Fulvic Acid in Waste Slurry on Flocculation and Zeta Potential. *Sustainability*, 13(14), 7784. doi:10.3390/su13147784.
- [28] Snellings, R., Horckmans, L., Van Bunderen, C., Vandewalle, L., & Cizer, Ö. (2017). Flash-calcined dredging sediment blended cements: effect on cement hydration and properties. *Materials and Structures/Materiaux et Constructions*, 50(6). doi:10.1617/s11527-017-1108-5.
- [29] Tironi, A., Trezza, M. A., Scian, A. N., & Irassar, E. F. (2012). Kaolinitic calcined clays: Factors affecting its performance as pozzolans. *Construction and Building Materials*, 28(1), 276–281. doi:10.1016/j.conbuildmat.2011.08.064.
- [30] Fernandez, R., Martirena, F., & Scrivener, K. L. (2011). The origin of the pozzolanic activity of calcined clay minerals: A comparison between kaolinite, illite and montmorillonite. *Cement and Concrete Research*, 41(1), 113–122. doi:10.1016/j.cemconres.2010.09.013.
- [31] Safhi, A. el M., Benzerzour, M., Rivard, P., Abriak, N. E., & Ennahal, I. (2019). Development of self-compacting mortars based on treated marine sediments. *Journal of Building Engineering*, 22, 252–261. doi:10.1016/j.jobe.2018.12.024.
- [32] Benzerzour, M., Amar, M., & Abriak, N.-E. (2017). New experimental approach of the reuse of dredged sediments in a cement matrix by physical and heat treatment. *Construction and Building Materials*, 140, 432–444. doi:10.1016/j.conbuildmat.2017.02.142.
- [33] Safhi, A. el M., Rivard, P., Yahia, A., Benzerzour, M., & Khayat, K. H. (2020). Valorization of dredged sediments in self-consolidating concrete: Fresh, hardened, and microstructural properties. *Journal of Cleaner Production*, 263. doi:10.1016/j.jclepro.2020.121472.
- [34] Amar, M., Benzerzour, M., Safhi, A. E. M., & Abriak, N. E. (2018). Durability of a cementitious matrix based on treated sediments. *Case Studies in Construction Materials*, 8, 258–276. doi:10.1016/j.cscm.2018.01.007.
- [35] Amar, M., Benzerzour, M., Abriak, N. E., & Mamindy-Pajany, Y. (2017). Study of the pozzolanic activity of a dredged sediment from Dunkirk harbour. *Powder Technology*, 320, 748–764. doi:10.1016/j.powtec.2017.07.055.
- [36] Bucher, R., Cyr, M., & Escadeillas, G. (2021). Performance-based evaluation of flash-metakaolin as cement replacement in marine structures—Case of chloride migration and corrosion. *Construction and Building Materials*, 267. doi:10.1016/j.conbuildmat.2020.120926.
- [37] San Nicolas, R., Cyr, M., & Escadeillas, G. (2013). Characteristics and applications of flash metakaolins. *Applied Clay Science*, 83–84, 253–262. doi:10.1016/j.clay.2013.08.036.
- [38] Chen, C., Habert, G., Bouzidi, Y., Jullien, A., & Ventura, A. (2010). LCA allocation procedure used as an incitative method for waste recycling: An application to mineral additions in concrete. *Resources, Conservation and Recycling*, 54(12), 1231–1240. doi:10.1016/j.resconrec.2010.04.001.
- [39] Zeraoui, A., Maherzi, W., Benzerzour, M., Abriak, N. E., & Aouad, G. (2023). Development of Flash-Calcined Sediment and Blast Furnace Slag Ternary Binders. *Buildings*, 13(2), 333. doi:10.3390/buildings13020333.
- [40] Alloul, A., Amar, M., Benzerzour, M., & Abriak, N. E. (2023). Developing mortar using limestone flash-calcined dredged sediment/millstone-clay cement binder (LFC). *Journal of Building Engineering*, 76. doi:10.1016/j.jobe.2023.107346.

- [41] Chu, D. C., Kleib, J., Amar, M., Benzerzour, M., & Abriak, N. E. (2022). Recycling of dredged sediment as a raw material for the manufacture of Portland cement – Numerical modeling of the hydration of synthesized cement using the CEMHYD3D code. *Journal of Building Engineering*, 48. doi:10.1016/j.job.2021.103871.
- [42] Chu, D. C., Kleib, J., Amar, M., Benzerzour, M., & Abriak, N. E. (2021). Determination of the degree of hydration of Portland cement using three different approaches: Scanning electron microscopy (SEM-BSE) and Thermogravimetric analysis (TGA). *Case Studies in Construction Materials*, 15. doi:10.1016/j.cscm.2021.e00754.
- [43] Schläpfer, P., & Bukowski, R. (1933). Studies on the determination of free lime and calcium hydroxide in cement clinkers, cements, and slags and set hydraulic mortars, Federal Materials Testing Institute at the E.T.H., 63, Zurich, German.
- [44] NF-EN 196-3. (2017). Methods of testing cement. Part 3: Determination of setting times and soundness. Association Française de Normalisation (AFNOR), Saint-Denis Cedex, France. (In French).
- [45] Chikouche, M. A., Ghorbel, E., & Bibi, M. (2016). The possibility of using dredging sludge in manufacturing cements: Optimization of heat treatment cycle and ratio replacement. *Construction and Building Materials*, 106, 330-341. doi:10.1016/j.conbuildmat.2015.12.128.
- [46] Beaudoin, J., & Odler, I. (2019). Hydration, Setting and Hardening of Portland Cement. *Lea's Chemistry of Cement and Concrete*, 157–250, Butterworth-Heinemann, Oxford, United Kingdom. doi:10.1016/b978-0-08-100773-0.00005-8.
- [47] Zhang, J., & Scherer, G. W. (2011). Comparison of methods for arresting hydration of cement. *Cement and Concrete Research*, 41(10), 1024–1036. doi:10.1016/j.cemconres.2011.06.003.
- [48] Scrivener, K., Snellings, R., & Lothenbach, B. (Eds.). (2018). *A Practical Guide to Microstructural Analysis of Cementitious Materials*. CRC Press, Boca Raton, United States. doi:10.1201/b19074.
- [49] Georget, F., Wilson, W., & Scrivener, K. L. (2021). EDXIA: Microstructure characterisation from quantified SEM-EDS hypermaps. *Cement and Concrete Research*, 141. doi:10.1016/j.cemconres.2020.106327.
- [50] NF EN 196-1. (2016). Methods of testing cement - Part 1: determination of strength. Association Française de Normalisation (AFNOR), Saint-Denis Cedex, France. (In French).
- [51] Rao, G. A. (2001). Generalization of Abrams' law for cement mortars. *Cement and Concrete Research*, 31(3), 495–502. doi:10.1016/S0008-8846(00)00473-7.
- [52] Lecomte, A., De Larrard, F., & Mechling, J. M. (2001). Compressive strength of hydraulic concretes to the unoptimised granular skeleton. *Bulletin LPC*, 234, 89-105. (In French).
- [53] Amar, M., Benzerzour, M., & Abriak, N. E. (2018). Towards the establishment of formulation laws for sediment-based mortars. *Journal of Building Engineering*, 16, 106–117. doi:10.1016/j.job.2017.12.011.
- [54] Lothenbach, B., Scrivener, K., & Hooton, R. D. (2011). Supplementary cementitious materials. *Cement and Concrete Research*, 41(12), 1244–1256. doi:10.1016/j.cemconres.2010.12.001.
- [55] Avet, F., & Scrivener, K. (2020). Effect of temperature on the water content of CASH in plain Portland and blended cements. *Cement and Concrete Research*, 136, 106124. doi:10.1016/j.cemconres.2020.106124.
- [56] Bouarroudj, M. E., Rémond, S., Bulteel, D., Potier, G., Michel, F., Zhao, Z., & Courard, L. (2021). Use of grinded hardened cement pastes as mineral addition for mortars. *Journal of Building Engineering*, 34, 101863. doi:10.1016/j.job.2020.101863.
- [57] Kocaba, V., Gallucci, E., & Scrivener, K. L. (2012). Methods for determination of degree of reaction of slag in blended cement pastes. *Cement and Concrete Research*, 42(3), 511–525. doi:10.1016/j.cemconres.2011.11.010.
- [58] Deboucha, W., Leklou, N., Khelidj, A., & Oudjit, M. N. (2017). Hydration development of mineral additives blended cement using thermogravimetric analysis (TGA): Methodology of calculating the degree of hydration. *Construction and Building Materials*, 146, 687–701. doi:10.1016/j.conbuildmat.2017.04.132.
- [59] NF EN 206-1. (2004). Concrete - Part 1: Specification, performance, production and conformity. Association Française de Normalisation (AFNOR), Saint-Denis Cedex, France. (In French).
- [60] Pane, I., & Hansen, W. (2005). Investigation of blended cement hydration by isothermal calorimetry and thermal analysis. *Cement and Concrete Research*, 35(6), 1155–1164. doi:10.1016/j.cemconres.2004.10.027.
- [61] NIST (2003). Technical Note VCCTL-01. National Institute of Standards and Technology, Maryland, United States. Available online: <https://nvlpubs.nist.gov/nistpubs/Legacy/IR/nistir7096.pdf> (accessed on May 2023).
- [62] Collepardi, M., Baldini, G., Pauri, M., & Corradi, M. (1978). The effect of pozzolanas on the tricalcium aluminate hydration. *Cement and Concrete Research*, 8(6), 741–751. doi:10.1016/0008-8846(78)90083-2.
- [63] Bentz, D. P., Ardani, A., Barrett, T., Jones, S. Z., Lootens, D., Peltz, M. A., Sato, T., Stutzman, P. E., Tanesi, J., & Weiss, W. J. (2015). Multi-scale investigation of the performance of limestone in concrete. *Construction and Building Materials*, 75, 1–10. doi:10.1016/j.conbuildmat.2014.10.042.

- [64] Bentz, D. P. (2006). Modeling the influence of limestone filler on cement hydration using CEMHYD3D. *Cement and Concrete Composites*, 28(2), 124–129. doi:10.1016/j.cemconcomp.2005.10.006.
- [65] Fernandez Lopez, R. (2009). Calcined clayey soils as a potential replacement for cement in developing countries. Ph.D. Thesis, Swiss Federal Institute of Technology Lausanne, Lausanne, Switzerland.
- [66] Hjorth, J., Skibsted, J., & Jakobsen, H. J. (1988). ²⁹Si MAS NMR studies of portland cement components and effects of microsilica on the hydration reaction. *Cement and Concrete Research*, 18(5), 789–798. doi:10.1016/0008-8846(88)90104-4.
- [67] Ramachandran, V. S. (1976). Hydration of cement—role of triethanolamine. *Cement and Concrete research*, 6(5), 623–631. doi:10.1016/0008-8846(76)90026-0.
- [68] Kolani, B., Buffo-Lacarrière, L., Sellier, A., Escadeillas, G., Boutillon, L., & Linger, L. (2012). Hydration of slag-blended cements. *Cement and Concrete Composites*, 34(9), 1009–1018. doi:10.1016/j.cemconcomp.2012.05.007.
- [69] Juenger, M. C., Snellings, R., & Bernal, S. A. (2019). Supplementary cementitious materials: New sources, characterization, and performance insights. *Cement and Concrete Research*, 122, 257–273. doi:10.1016/j.cemconres.2019.05.008.
- [70] Zajac, M., Rossberg, A., Le Saout, G., & Lothenbach, B. (2014). Influence of limestone and anhydrite on the hydration of Portland cements. *Cement and Concrete Composites*, 46, 99–108. doi:10.1016/j.cemconcomp.2013.11.007.
- [71] Okoronkwo, M. U., & Glasser, F. P. (2016). Stability of strätlingite in the CASH system. *Materials and Structures/Materiaux et Constructions*, 49(10), 4305–4318. doi:10.1617/s11527-015-0789-x.
- [72] Bahman-Zadeh, F., Ramezani-pour, A. A., & Zolfagharnasab, A. (2022). Effect of carbonation on chloride binding capacity of limestone calcined clay cement (LC3) and binary pastes. *Journal of Building Engineering*, 52. doi:10.1016/j.job.2022.104447.
- [73] Mokhtar, M., Inayat, A., Ofili, J., & Schwieger, W. (2010). Thermal decomposition, gas phase hydration and liquid phase reconstruction in the system Mg/Al hydrotalcite/mixed oxide: A comparative study. *Applied Clay Science*, 50(2), 176–181. doi:10.1016/j.clay.2010.07.019.
- [74] Ye, H., Huang, L., & Chen, Z. (2019). Influence of activator composition on the chloride binding capacity of alkali-activated slag. *Cement and Concrete Composites*, 104, 103368. doi:10.1016/j.cemconcomp.2019.103368.
- [75] Cardinaud, G., Rozière, E., Martinage, O., Loukili, A., Barnes-Davin, L., Paris, M., & Deneele, D. (2021). Calcined clay – Limestone cements: Hydration processes with high and low-grade kaolinite clays. *Construction and Building Materials*, 277. doi:10.1016/j.conbuildmat.2021.122271.
- [76] Avet, F., & Scrivener, K. (2018). Investigation of the calcined kaolinite content on the hydration of Limestone Calcined Clay Cement (LC3). *Cement and Concrete Research*, 107, 124–135. doi:10.1016/j.cemconres.2018.02.016.
- [77] Antoni, M., Rossen, J., Martirena, F., & Scrivener, K. (2012). Cement substitution by a combination of metakaolin and limestone. *Cement and Concrete Research*, 42(12), 1579–1589. doi:10.1016/j.cemconres.2012.09.006.
- [78] Wang, D., Shi, C., Farzadnia, N., Shi, Z., Jia, H., & Ou, Z. (2018). A review on use of limestone powder in cement-based materials: Mechanism, hydration and microstructures. *Construction and Building Materials*, 181, 659–672. doi:10.1016/j.conbuildmat.2018.06.075.
- [79] Alarcon-Ruiz, L., Platret, G., Massieu, E., & Ehrlicher, A. (2005). The use of thermal analysis in assessing the effect of temperature on a cement paste. *Cement and Concrete Research*, 35(3), 609–613. doi:10.1016/j.cemconres.2004.06.015.
- [80] Castellote, M., Alonso, C., Andrade, C., Turrillas, X., & Campo, J. (2004). Composition and microstructural changes of cement pastes upon heating, as studied by neutron diffraction. *Cement and Concrete Research*, 34(9), 1633–1644. doi:10.1016/S0008-8846(03)00229-1.
- [81] Zhang, Y., & Çopuroğlu, O. (2022). The role of hydrotalcite-like phase and monosulfate in slag cement paste during atmospheric and accelerated carbonation. *Cement and Concrete Composites*, 132. doi:10.1016/j.cemconcomp.2022.104642.
- [82] Mounanga, P., Khelidj, A., Loukili, A., & Baroghel-Bouny, V. (2004). Predicting Ca(OH)₂ content and chemical shrinkage of hydrating cement pastes using analytical approach. *Cement and Concrete Research*, 34(2), 255–265. doi:10.1016/j.cemconres.2003.07.006.
- [83] Snellings, R., Machner, A., Bolte, G., Kamyab, H., Durdzinski, P., Teck, P., Zajac, M., Muller, A., de Weerd, K., & Haha, M. Ben. (2022). Hydration kinetics of ternary slag-limestone cements: Impact of water to binder ratio and curing temperature. *Cement and Concrete Research*, 151. doi:10.1016/j.cemconres.2021.106647.
- [84] Taylor, R., Richardson, I. G., & Brydson, R. M. D. (2010). Composition and microstructure of 20-year-old ordinary Portland cement-ground granulated blast-furnace slag blends containing 0 to 100% slag. *Cement and Concrete Research*, 40(7), 971–983. doi:10.1016/j.cemconres.2010.02.012.
- [85] Muller, A. C. A. (2014). Characterization of porosity & CSH in cement pastes by ¹H NMR. Ph.D. Thesis, Swiss Federal Institute of Technology Lausanne, Lausanne, Switzerland.

- [86] Rossen, J. E., & Scrivener, K. L. (2017). Optimization of SEM-EDS to determine the C–A–S–H composition in matured cement paste samples. *Materials Characterization*, 123, 294–306. doi:10.1016/j.matchar.2016.11.041.
- [87] Gruskovnjak, A., Lothenbach, B., Holzer, L., Figi, R., & Winnefeld, F. (2006). Hydration of alkali-activated slag: comparison with ordinary Portland cement. *Advances in Cement Research*, 18(3), 119–128. doi:10.1680/adcr.2006.18.3.119.
- [88] Bazzoni, A., Suhua, M., Wang, Q., Shen, X., Cantoni, M., & Scrivener, K. L. (2014). The effect of magnesium and zinc ions on the hydration kinetics of C3S. *Journal of the American Ceramic Society*, 97(11), 3684–3693. doi:10.1111/jace.13156.
- [89] Yudenfreund, M., Odler, I., & Brunauer, S. (1972). Hardened portland cement pastes of low porosity I. Materials and experimental methods. *Cement and Concrete Research*, 2(3), 313–330. doi:10.1016/0008-8846(72)90073-7.
- [90] Cassagnabère, F., Mouret, M., & Escadeillas, G. (2009). Early hydration of clinker-slag-metakaolin combination in steam curing conditions, relation with mechanical properties. *Cement and Concrete Research*, 39(12), 1164–1173. doi:10.1016/j.cemconres.2009.07.023.
- [91] Lawrence, P., Cyr, M., & Ringot, E. (2003). Mineral admixtures in mortars: Effect of inert materials on short-term hydration. *Cement and Concrete Research*, 33(12), 1939–1947. doi:10.1016/S0008-8846(03)00183-2.
- [92] Papayianni, I., & Stefanidou, M. (2006). Strength-porosity relationships in lime-pozzolan mortars. *Construction and Building Materials*, 20(9), 700–705. doi:10.1016/j.conbuildmat.2005.02.012.
- [93] Chabannes, M., Kazemi-Kamyab, H., Trigallez, J., & Snellings, R. (2022). Performance and microstructure development of lime–calcined fluvial sediment binders under different curing conditions. *Cement and Concrete Research*, 160, 106903. doi:10.1016/j.cemconres.2022.106903.
- [94] Du, H., & Pang, S. D. (2020). High-performance concrete incorporating calcined kaolin clay and limestone as cement substitute. *Construction and Building Materials*, 264. doi:10.1016/j.conbuildmat.2020.120152.
- [95] Cheng, S., Shui, Z., Sun, T., Yu, R., & Zhang, G. (2018). Durability and microstructure of coral sand concrete incorporating supplementary cementitious materials. *Construction and Building Materials*, 171, 44–53. doi:10.1016/j.conbuildmat.2018.03.082.